

1  
2 **A Model-Independent Data Assimilation (MIDA) module and its applications in ecology**

3  
4 Xin Huang<sup>1,2</sup>, Dan Lu<sup>3</sup>, Daniel M. Ricciuto<sup>4</sup>, Paul J. Hanson<sup>4</sup>, Andrew D. Richardson<sup>1,2</sup>, Xuehe  
5 Lu<sup>5</sup>, Ensheng Weng<sup>6,7</sup>, Sheng Nie<sup>8</sup>, Lifen Jiang<sup>1</sup>, Enqing Hou<sup>1</sup>, Igor F. Steinmacher<sup>2</sup>, Yiqi  
6 Luo<sup>1,2,9</sup>

7  
8 1 Center for Ecosystem Science and Society, Northern Arizona University, Flagstaff, AZ, USA  
9 2 School of informatics, Computing, and Cyber Systems, Northern Arizona University, Flagstaff,  
10 AZ, USA

11 3 Computational Sciences and Engineering Division, Climate Change Science Institute,  
12 Oak Ridge National Laboratory, Oak Ridge, TN, USA

13 4 Environmental Sciences Division, Climate Change Science Institute, Oak Ridge National  
14 Laboratory, Oak Ridge, TN, USA

15 5 International Institute for Earth System Science, Nanjing University, Nanjing, China

16 6 Center for Climate Systems Research, Columbia University, New York, USA

17 7 NASA Goddard Institute for Space Studies, New York, USA

18 8 Key Laboratory of Digital Earth Science, Aerospace Information Research Institute, Chinese  
19 Academy of Sciences, Beijing, China

20 9 Department of Biological Sciences, Northern Arizona University, Flagstaff, AZ, USA

21

22 *Correspondence to:* Xin Huang ([xh59@nau.edu](mailto:xh59@nau.edu))

23

24 **ABSTRACT**

25 Models are an important tool to predict Earth system dynamics. An accurate prediction of future  
26 states of ecosystems depends on not only model structures but also parameterizations. Model  
27 parameters can be constrained by data assimilation. However, applications of data assimilation to  
28 ecology are restricted by highly technical requirements such as model-dependent coding. To  
29 alleviate this technical burden, we developed a model-independent data assimilation (MIDA)  
30 module. MIDA works in three steps including data preparation, execution of data assimilation,  
31 and visualization. The first step prepares prior ranges of parameter values, a defined number of  
32 iterations, and directory paths to access files of observations and models. The execution step  
33 calibrates parameter values to best fit the observations and estimates the parameter posterior  
34 distributions. The final step automatically visualizes the calibration performance and posterior  
35 distributions. MIDA is model independent and modelers can use MIDA for an accurate and  
36 efficient data assimilation in a simple and interactive way without modification of their original  
37 models. We applied MIDA to four types of ecological models: the data assimilation linked  
38 ecosystem carbon (DALEC) model, a surrogate-based energy exascale earth system model: the  
39 land component (ELM), nine phenological models and a stand-alone biome ecological strategy  
40 simulator (BiomeE). The applications indicate that MIDA can effectively solve data assimilation  
41 problems for different ecological models. Additionally, the easy implementation and model-  
42 independent feature of MIDA breaks the technical barrier of applications of data-model fusion in  
43 ecology. MIDA facilitates the assimilation of various observations into models for uncertainty  
44 reduction in ecological modeling and forecasting.

45 **Keywords:**

46 Parameter uncertainty quantification, Data assimilation, Modules, Ecological models

47 **1. Introduction**

48 Ecological models require a large number of parameters to simulate biogeophysical and  
49 biogeochemical processes (Bonan, 2019; Ciais et al., 2013; Friedlingstein et al., 2006), and  
50 specify model behaviors (Luo et al., 2016; Luo and Schuur, 2020). Parameter values in  
51 ecological models are mostly determined in some *ad hoc* fashions (Luo et al., 2001), leading to  
52 considerable biases in predictions (Tao et al., 2020). The situation becomes even worse when  
53 more detailed processes are incorporated into models (De Kauwe et al., 2017; Lawrence et al.,  
54 2019). Data assimilation (DA), a statistically rigorous method to integrate observations and  
55 models, is gaining increasing attention for parameter estimation and uncertainty evaluation. It  
56 has been successfully applied to many ecological models (Fox et al., 2009; Keenan et al., 2012;  
57 Richardson et al., 2010; Safta et al., 2015; Wang et al., 2009; Williams et al., 2005; Zobitz et al.,  
58 2011). However, almost all those DA studies require model-dependent, invasive coding (Walls et  
59 al., 2005). This requires a DA algorithm to be programmed for a specific model. Such model-  
60 dependent coding creates a large technical barrier for ecologists to use DA to solve prediction  
61 and uncertainty quantification problems in ecology. Thus a model-independent DA toolkit is  
62 required to facilitate the use of DA technique in ecology.

63 DA is a powerful approach to combine models with observations and can be used to  
64 improve ecological research in several ways (Luo et al., 2011). First, DA can be used for  
65 parameter estimation (Bloom et al., 2016; Hararuk et al., 2015; Hou et al., 2019; Ise and  
66 Moorcroft, 2006; Ma et al., 2017; Ricciuto et al., 2011; Scholze et al., 2007). It enables the  
67 optimization of parameter values across sites, time and treatments (Li et al., 2018; Luo and  
68 Schuur, 2020). For example, Hararuk and his colleagues applied DA to a global land model and  
69 substantially improved the explanability of the global variation in soil organic carbon (SOC)

70 from 27% to 41% (Hararuk et al., 2014). When DA was combined with deep learning to improve  
71 spatial distributions of estimated parameter values, for example, the Community Land Model  
72 version 5 (CLM5) predicted the SOC distribution in the US continent with much higher  $R^2$  of  
73 0.62 than CLM5 with default parameters ( $R^2 = 0.32$ ) (Tao et al., 2020). Second, DA can be used  
74 to select alternative model structures to better represent ecological processes (Liang et al., 2018;  
75 Van Oijen et al., 2011; Shi et al., 2018; Smith et al., 2013; Williams et al., 2009). In the study by  
76 Liang et al. (2018), DA was used to evaluate four models. And a two-pool interactive model was  
77 selected after DA to best represent SOC decomposition with priming. Additionally, DA can be  
78 applied to locate the most informative data to reduce uncertainty, thus guiding the sensor  
79 network design. (Keenan et al., 2013; Raupach et al., 2005; Shi et al., 2018; Williams et al.,  
80 2005). One DA study at Harvard Forest (Keenan et al., 2013) indicated that only a few data  
81 sources contributed to the significant reduction in parameter uncertainty. In spite of powerful  
82 applications of DA to ecological research, computational cost is a major hurdle, especially with  
83 complex models. Fer et al. (2018) developed a Bayesian model emulation to reduce the time cost  
84 of DA from 112h to 6h with the simplified Photosynthesis and Evapotranspiration model.  
85 Overall, DA is essential for ecological modeling and forecasting (Jiang et al., 2018) and is  
86 helpful for evaluation of different inversion methods (Fox et al., 2009).

87 Applications of traditional DA to ecological research require highly technical skills of  
88 users. A successful DA application usually involves model-dependent coding to integrate  
89 observations into models. This requires users to have knowledge about model programing. For  
90 example, if a complex model (e.g., the community land model) is used in DA, users need to  
91 know the programming language (e.g., Fortran) of the model and its internal content to write DA  
92 algorithm into the model source code before DA can be conducted. The learning curve for model

93 programing is steep for general ecologists. Furthermore, users often need to update the  
94 programming knowledge when a different model is used in DA. For example, scientists who  
95 implemented the DA algorithm coded in MATLAB ( Xu et al., 2006) to an ecosystem carbon  
96 cycle model programmed in Fortran (e.g., TECO) need to understand both MATLAB and  
97 Fortran (Ma et al., 2017). Moreover, DA often involves reading observation files about a specific  
98 study site. As a result, users usually have to update the codes of model-dependent DA to read  
99 new observations from every new study site.

100 A number of tools have been developed to facilitate DA applications (Table 1) but many  
101 of them are model dependent, such as the Carbon Cycle Data Assimilation Systems (CCDAS)  
102 (Rayner et al., 2005; Scholze et al., 2007), the Carbon Data Model Framework (CARDAMOM)  
103 (Bloom et al., 2016), the Ecological Platform for Assimilating Data (EcoPAD) into model  
104 (Huang et al. 2019) and Predictive Ecosystem Analyzer (PEcAn) (LeBauer et al., 2013). These  
105 tools combine DA algorithms with a specific model. For example, CCDAS specified the DA  
106 algorithm to the Biosphere Energy Transfer Hydrology (BETHY) model (Rayner et al., 2005).  
107 The hardcoding feature of aforementioned tools make them inflexible to be applied to different  
108 models.

109 There are some model independent DA tools that are not tailored to a specific model,  
110 such as Data Assimilation Research Testbed (DART) (Anderson et al., 2009), the open Data  
111 Assimilation library (openDA) (Ridler et al., 2014), the Parallel Data Assimilation Framework  
112 (PDAF) (Nerger and Hiller, 2013) and Parameter Estimation & Uncertainty Analysis software  
113 suit (PEST) (Doherty, 2004).

114 However, these model-independent tools suffer from some limitations for a general and  
115 flexible DA application. For example, openDA requires users to code three functions to initialize

116 a Java class (Ridler et al., 2014) (Table 1). DART enables incorporating a new model through a  
117 range of interfaces (Anderson et al., 2009). It has been successfully applied to atmospheric and  
118 oceanic models with currently available interfaces (Anderson et al., 2009; Raeder et al., 2012)  
119 and recently to the community land model (Fox et al., 2018). It is likely that users may need to  
120 prepare new interfaces for new ecological models to use DART. DART and PDAF adopted the  
121 Ensemble Kalman Filter (EnKF) method (Evensen, 2003), which may makes it difficult to obey  
122 mass conservation for biogeochemical models. This is because the parameter values estimated by  
123 EnKF change each time when new data sets are assimilated (Allen et al., 2003; Gao et al., 2011;  
124 Trudinger et al., 2007). The sudden changes in estimated parameter values at time points when  
125 data are assimilated by EnKF usually do not reflect reality of biogeochemical cycles in the real  
126 world. PEST utilizes Levenberg-Marquardt method (Levenberg, 1944) which is a local  
127 optimization method for parameter estimation. If the relationship between simulation outputs and  
128 parameters are highly nonlinear, which is common in ecological models, this method may trap  
129 into a locally optimization solution (Doherty, 2004).

130 In this work, we developed a model-independent DA module (MIDA) to enable a general  
131 and flexible application of DA in ecology. MIDA was designed as a highly modular tool,  
132 independent of specific models, and friendly to users with limited programming skills and/or  
133 technical knowledge of DA algorithms. Additionally, MIDA implemented advanced Markov  
134 Chain Monte Carlo (MCMC) algorithms for DA analysis which can accurately quantify the  
135 parameter uncertainty with informative posterior distribution. The anticipated user community in  
136 this initial phase of MIDA development is the biogeochemical modelers who are looking for  
137 appropriate parameter estimation methods. In the following Section 2, we first introduce the  
138 development details of MIDA and its usage. In Section 3, we demonstrate the application of

139 MIDA to four different types of ecological models. In Section 4, we discuss the strengths and  
140 weaknesses of MIDA in ecological modelling and lastly we give our concluding remarks in  
141 Section 5.

142

143 **2. Model-independent data assimilation (MIDA)**

144 **2.1 Bayes's theorem and DA**

145 Based on Bayes' theorem, DA is a statistical approach to constrain parameter values and  
146 estimate their posterior density distributions through assimilating observations into a model. The  
147 posterior density distributions  $p(C|Z)$  of parameters  $C$  for a given observation  $Z$  can be obtained  
148 from *prior* density distributions  $p(C)$  and the likelihood function  $p(Z|C)$ :

$$149 \quad p(C|Z) \propto p(Z|C)p(C) \quad (1)$$

150 The *prior* density distribution  $p(C)$  is assumed as a uniform distribution over the parameter  
151 range. And the likelihood function is negatively proportional to a cost function,  $J$  as:

$$152 \quad p(Z|C) \propto \exp(-J) \quad (2)$$

153 The cost function measures the misfit between simulation outputs and observations and is  
154 described in more detail in section 2.4. The posterior density distributions  $p(C|Z)$  is estimated  
155 from sampling parameter values to maximize the likelihood function  $p(Z|C)$  or minimize the  
156 cost function  $J$ . DA usually uses a sampling technique, such as Markov chain Monte Carlo  
157 (MCMC) in this MIDA. The MCMC algorithm successively generates a new set of parameter  
158 values from the prior parameter ranges and requires model run with these new parameter values.  
159 Then the cost function is calculated to determine whether this new set of parameter values will  
160 be accepted or not according to the Metropolis-Hastings criterion (see more description in  
161 section 2.4). All accepted parameter values are used to generate posterior distributions where the

162 distinctive mode indicates the parameter uncertainty is well constrained. Meanwhile, we derive  
163 maximum likelihood estimates (MLEs) of parameters from the posterior density distributions.

164 MIDA realizes model-independent Bayesian-based DA to estimate posterior density  
165 distributions and MLEs of parameters via data exchanges between a given model and DA  
166 algorithm.

167

## 168 **2.2 An overview of MIDA**

169 MIDA is a module that allows for automatic implementation of data assimilation without  
170 intrusive modification or coding of the original model (<https://doi.org/10.5281/zenodo.4762725>,  
171 last access: May 2021). Its workflow includes three steps: data preparation, execution of data  
172 assimilation, and visualization (Fig. 1). Step 1 (data preparation) is to establish the standardized  
173 data exchange between DA algorithm and the model. Step 2 (execution of data assimilation) is to  
174 run DA as a black box independent of the model. Step 3 (visualization) is to diagnose parameter  
175 uncertainty after DA. The modularity of the 3-step workflow is designed to enable MIDA for a  
176 rapid DA application and adaption to a new model. In the following, we introduce the three-step  
177 workflows of MIDA, its technical implementation and usage in detail.

178

## 179 **2.3 Step 1: Data preparation**

180 Step 1 is designed to initialize data exchange to transfer parameter values, model outputs,  
181 observations and their variances between DA algorithm and the model to be used. Four types of  
182 information are required either from interactive input or by modifying the ‘namelist.txt’ file (Fig.  
183 1). The first type is about DA configuration, including the number of sampling series in DA and  
184 the working path where the outputs of DA will be saved. The number of a sampling series is

185 essential in a DA task to define how many times parameter values are sampled to run the model.  
186 The second type of information is about parameter ranges and their covariance. The third is the  
187 model executable file. Finally, the fourth type is an output configuration file which contains the  
188 file paths of model outputs, observations, and their variance. This file also instructs how to read  
189 model outputs and compare each output with corresponding observation.

190 Traditional DA requires users to modify the code of model to incorporate the process of  
191 data exchange between DA algorithm and the model. Therefore, the program of data exchange in  
192 traditional DA is model-specific and users need to repeat such program when a new model  
193 comes. In MIDA, the process of data exchange calls a model executable file which hides the  
194 details of model code. When applied to a new model, MIDA only requires users to provide a  
195 different model executable file in the ‘namelist.txt’ file and does not involve any additional  
196 coding in either the model or MIDA. Thus, MIDA lowers the technical barrier for general  
197 ecologists to conduct DA.

198 Traditional DA usually preset the number of parameters and the model outputs according  
199 to a specific model before initializing the data exchange. This is because data exchange between  
200 DA algorithm and model uses memory to transfer items such as parameter values. Instead,  
201 MIDA organizes items in data exchange using different files. Items in data exchange are decided  
202 by the data file loaded when MIDA is running. The number of parameter values, for example,  
203 will be decided after the file of parameter range is read in MIDA. Through modifying files,  
204 MIDA allows making efficient choices about the model-related items in data exchange. Thus,  
205 MIDA is highly flexible and modular for DA with different models.

206 Traditional DA also preset observation types in the data exchange according to a specific  
207 study before the data exchange. For example, if the traditional DA uses carbon flux observation,

208 it cannot switch to satellite remote sensing products without additional coding. MIDA uses the  
209 concepts of object-orient programming (Mitchell and Apt, 2003) and dynamic initialization  
210 (Cline et al., 1998) in computer science to provide a homogenous way to create various  
211 observation types from a unified prototype class. A prototype class includes variables to store  
212 observations and their variance and functions (e.g., read from observation files). The values in  
213 variables are dynamically decided after the observation files are loaded when MIDA is running.  
214 Different observation types derive from the prototype class with a high degree of reusability of  
215 most functions. In such way, MIDA only requires users to provide different filenames of the  
216 observations to be integrated in DA. Therefore, MIDA is highly flexible and modular for DA to  
217 assimilate various observations.

218

## 219 **2.4 Step 2: Execution of data assimilation**

220 After the establishment of the standardized data exchange (step 1), step 2 is to run DA as a black  
221 box for users without knowledge of DA itself. Notwithstanding the black-box goal, this section  
222 provides a general description of DA below.

223 Data assimilation as a process integrates observations into a model to constrain  
224 parameters and estimate parameter uncertainties. Data assimilation usually uses some types of  
225 sampling algorithms, such as Markov chain Monte Carlo (MCMC), to generate posterior  
226 parameter distribution under a Bayesian inference framework (Box and Tiao, 1992). As  
227 mentioned in section 2.1, DA with MCMC algorithm estimates the posterior density distributions  
228 through sampling to maximize likelihood function  $p(Z|C)$  or minimize the misfit  $J$  between  
229 simulation outputs and observations. This version of MIDA uses MCMC algorithm implemented  
230 by the Metropolis-Hasting (MH) sampling method (Hastings, 1970; Metropolis et al., 1953). The

231 future version of MIDA could incorporate other data assimilation algorithms. Each iteration in  
 232 the Metropolis-Hasting sampling includes a proposing phase and a moving phase. The proposing  
 233 phase generates a new set of parameter values based on the starting point for the first iteration or  
 234 current accepted parameter values in the following iterations. If parameter covariance  
 235 ( $cov_{param}$ ) is specified in step 1 on data preparation, this proposing phase will draw new  
 236 parameter values ( $C_{new}$ ) within the prior ranges from a Gaussian distribution  $N(C_{old}, cov_{param})$   
 237 where  $C_{old}$  is the predecessor set of parameter values. Without parameter covariance, new set of  
 238 parameter values will be generated from a uniform distribution within the prior ranges (Xu et al.,  
 239 2006).

240 The moving phase first calculates mismatches between observations and the model  
 241 simulation with the new set of parameter values as a cost function ( $J_{new}$  in Eq.3) (Xu et al.  
 242 2006):

$$243 J_{new} = \sum_{i=1}^n \frac{\sum_{t \in obs(Z_i)} [Z_i(t) - X_i(t)]^2}{2\sigma_i^2} \quad (3)$$

244 Where  $n$  is the number of observations,  $Z_i(t)$  is the  $i^{\text{th}}$  observation at time  $t$ ,  $X_i(t)$  is the  
 245 corresponding simulation,  $\sigma_i^2$  is the variance of the observation. The error is assumed to  
 246 independently follow a Gaussian distribution. This new set of parameter values will be accepted  
 247 if  $J_{new}$  is smaller than  $J_{old}$ , the cost function with the previous set of accepted parameter values,  
 248 or the value,  $\exp\left(-\frac{J_{new}}{J_{old}}\right)$ , is larger than a random number selected from a uniform distribution  
 249 from 0 to 1 according to the Metropolis criterion (Liang et al., 2018; Luo et al., 2011; Shi et al.,  
 250 2018; Xu et al., 2006). Once the new set of parameter values is accepted,  $J_{new}$  becomes  $J_{old}$ .  
 251 Those two phases of sampling will be iteratively executed until the number of sampling series set

252 in step 1 on preparation of DA is reached. Finally, the posterior density distributions can be  
253 generated from all the accepted parameter values.

254 MIDA realizes the execution of data assimilation according to the procedure described  
255 above. First, MIDA uses a ‘call’ function to execute model simulations to get values of  $X_i(t)$ .  
256 Observations  $Z_i(t)$  and their variance  $\sigma_i^2$  are already provided via the standardized data  
257 exchange as described in step 1. Then, MIDA calculates  $J_{new}$  according to Eq. 3 to decide the  
258 acceptance of the current parameter values used in this simulation. If accepted, MIDA saves this  
259 set of parameter values and associated  $J_{new}$  values in  $C_{accepted}$  and  $J_{accepted}$  arrays respectively  
260 and triggers new proposing phrase based on this set of accepted parameter values. If not, MIDA  
261 discards this set of parameter values and generates another new set of parameter values. MIDA  
262 saves the new parameter values generated in the proposing phrase to “ParameterValue.txt”, from  
263 which the model reads before execution of the next model simulation. MIDA repeats the  
264 proposing and moving phases until the number of sampling series is reached. At the end, MIDA  
265 selects the best parameter values through maximum likelihood estimation and run model again  
266 using this set of values to get optimized simulation outputs  $X_i(t)$ . Then MIDA saves the arrays  
267 of accepted parameters, associated errors, maximum likelihood estimates (MLEs), and optimized  
268 state variables  $X_i(t)$  to four files, “parameter\_accepted.txt”, “J\_accepted.txt”, “MLE.txt”, and  
269 “OptimizedSimu.txt”, respectively.

270 This execution of DA algorithm in MIDA enables users to conduct DA as a black box  
271 and is independent of any particular model.

272

273 **2.5 Step 3: Visualization**

274 Step 3 is to visualize the results of DA in step 2. The end products of DA are accepted parameter  
275 values, their associated  $J_{new}$  values, the maximum likelihood estimates, and optimized  
276 simulation results as saved in the output files. MIDA enables visualization of parameter posterior  
277 density distributions with a Python script. In the script, MIDA first read accepted parameter  
278 values from “parameter\_accepted.txt” file. Then, MIDA generates posterior probabilistic density  
279 function (PPDF) for each parameter via ‘kdeplot’ function in the ‘seaborn’ package. The  
280 maximum likelihood estimates of parameters correspond to the peaks of PPDF. The distinctive  
281 mode of PPDF indicates how well the parameter uncertainty is constrained. Finally, MIDA  
282 visualizes the PPDF for all parameters in a figure using the ‘matplotlib’ package.

283

## 284 **2.6 Implementation and architecture of MIDA**

285 MIDA is equipped with a graphical user interface (GUI) and users can easily execute it through  
286 an interactive window. Users can also run MIDA as a script program without the GUI. MIDA is  
287 written in Python (version 3.7). For the GUI-version, all relevant Python packages used in MIDA  
288 are compiled together, thus users do not need to install them by themselves. For the non-GUI  
289 version, users need to install Python 3.7 and relevant packages (i.e., numpy, pandas, shutil,  
290 subprocess, matplotlib, math, os, and seaborn). MIDA is compatible with model source codes  
291 written in multiple programming language (e.g., Fortran, C/C++, C#, MATLAB, R, or Python).  
292 It is also independent of multiple operation systems (e.g., Windows, Linux, MacOS). In addition,  
293 MIDA is also able to run on high-performance computing (HPC) platforms via task management  
294 systems (e.g., Slurm).

295 The architecture of MIDA is class-based and each class is designed to describe an object  
296 (e.g., parameter, observations, etc.) with variables and operations. Five classes are defined in

297 MIDA: parameter, observation, initialization, MCMC algorithm and the main program. The  
298 main program is the start of MIDA execution. It calls functions from all other classes to finish  
299 three-step workflow. As described in section 2.2, parameter and observation classes contain  
300 variables to be transferred in data exchanges via file I/O operations. These operations are  
301 implemented using the ‘numpy’ package. The initialization class is to read ‘namelist.txt’ in step  
302 1 on data preparation and to assign values for the variables in all other classes. Then the class of  
303 MCMC algorithm conducts DA as described in step 2. In this step, the simulation operation uses  
304 a ‘call’ function in ‘subprocess’ package to call model executable. At the start of model  
305 simulation, MIDA writes new parameter values to the ‘ParameterValue.txt’ file in the ‘working  
306 path’ directory specified in step 1 on data preparation. Then the model executable read parameter  
307 values from the ‘ParameterValue.txt’ file and run. After model simulation, DA algorithm can  
308 read the model outputs by the output filenames indicated in the output configuration file. After  
309 DA, step 3 executes an additional Python script to read accepted parameter values and plot the  
310 posterior density distributions of parameters. The plotting operations uses ‘matplotlib’ and  
311 ‘seaborn’ packages. The implementation of GUI uses pyQt5 toolkit to support interactive usage  
312 of MIDA. Users can also run MIDA in a non-interactive way with a ‘main.py’ script to trigger  
313 the three-step workflows.

314

## 315 **2.7 User information of MIDA**

316 In order to use MIDA, users need to prepare data and a model. The data to be used in MIDA are  
317 prior ranges and default values of parameters, parameter covariances, output configuration file,  
318 observations and their variances. They are organized in different files. Before running MIDA,  
319 users need to specify their filenames as suggested in step 1. When users want to use different

320 data sets in DA, they can simply change filenames with the new data sets via GUI or in the  
321 ‘namelist.txt’ file. Figure C1 is an example of the ‘namelist.txt’ file for a data assimilation study  
322 with the DALEC model. The model to be used in MIDA should have those to-be-estimated  
323 parameter values not fixed in model source code rather than changeable through  
324 ‘ParameterValue.txt’ file. MIDA writes new parameter values in each proposing phase during  
325 DA to the ‘ParameterValue.txt’ file, from which the model reads the parameter values to run the  
326 simulation.

327 To calculate the cost function,  $J$ , we have to have a one-to-one match between  
328 observations and model outputs. For example, phenology models in one of the application cases  
329 of MIDA below generate discrete dates of leaf onset, which is a one-to-one match to the  
330 observations of spring leaf onset. In this case, observation  $Z_i(t)$  and model output  $X_i(t)$  to be  
331 used in calculation of  $J$  is straightforward. In the application case for dynamic vegetation, the  
332 data to be used are leaf area in six layers in a forest of 302 years old whereas the model simulates  
333 leaf areas in eight layers from 0 to 800 years. To match observation, the model generates outputs  
334 of leaf areas in six layers when simulated forest age reaches 302 years. This requires users to  
335 prepare an output configuration file to instruct MIDA to read model outputs and re-organize their  
336 outputs to match observation. The output configuration file starts with a single line listing an  
337 observation filename and its corresponding output filenames. Content after the directories in the  
338 output configuration file are instructions to map model outputs with the observation signified in  
339 the first line. Each instruction is to match one or continuous elements in observation with  
340 elements in outputs with the same length. A blank line means there are no further instructions.  
341 Then a new matching between another observation and model outputs starts. An example of  
342 output configure file is available in Appendix B.

343       Once MIDA finishes the execution of data assimilation, users may need basic knowledge  
344      to assess the performance of DA. For example, the acceptance rate, which is given by MIDA, is  
345      the fraction of proposed parameter values that is accepted. Ideally, the acceptance rate should be  
346      about 20 ~ 50% (Xu et al., 2006). A very low acceptance rate indicates that many new proposed  
347      parameter values ( $C_{new}$ ) are rejected because  $C_{new}$  jumps too far away from the previously  
348      accepted parameter values (Robert and Casella, 2013; Roberts et al., 1997). In this case, users are  
349      suggested to reduce a jump scale in the proposing phase. On the other hand, a very high  
350      acceptance rate is likely because  $C_{new}$  moves slowly from the previously accepted parameter  
351      values. Users may increase the jump scale.

352       In addition, DA usually requires a convergence test to examine whether posterior  
353      distributions from different sampling series converge or not. Convergence test requires running  
354      DA parallelly or in multiple times with different initial parameter values. MIDA provides a  
355      Gelman-Rubin (G-R) test (Gelman and Rubin, 1992) for this purpose. To use the G-R test, users  
356      need to prepare a file containing initial parameters values in different sampling series and  
357      indicate its filename in the ‘namelist.txt’ file as described in step 1. If the G-R statistics  
358      approaches one, the sampling series in DA is converged. When sampling series is converged, all  
359      accepted parameter values are used to generate the posterior distributions.

360       There are three types of posterior distributions: bell-shape, edge-hitting, and flat. The  
361      bell-shaped posterior distributions indicate that these parameters are well constrained. Their peak  
362      values are the maximum likelihood estimates of parameter values. The flat posterior distributions  
363      suggest that the parameters are not constrained due to the lack of relevant information in data.  
364      The edge-hitting posterior distributions result from complex reasons, such as improper prior

365 parameter range. Users may change the prior ranges to examine if those posterior distributions  
366 can be improved or examine correlations among estimated parameters.

367

### 368 **3. Applications of MIDA**

369 We applied MIDA to four groups of models, which are an ecosystem carbon cycle model, a  
370 surrogate-based land surface model, nine phenology models, and a dynamic vegetation model,  
371 respectively. These four cases demonstrate that MIDA is effective for stand-alone DA, flexible  
372 to be applied to different models, and efficient for multiple model comparison.

#### 373 **3.1 Case 1: Independent data assimilation with DALEC**

374 The first case study is to demonstrate that MIDA can be effective for independent data  
375 assimilation with the data assimilation linked ecosystem carbon (DALEC) model (Lu et al.,  
376 2017). DALEC has been used for data assimilation in several studies (Bloom et al., 2016; Lu et  
377 al., 2017; Richardson et al., 2010; Safta et al., 2015; Williams et al., 2005). Previous studies all  
378 incorporated data assimilation algorithms into DALEC, which requires invasive coding. This  
379 case study is focused on reproducing the data assimilation results as in the study by Lu et al.  
380 (2017) but with MIDA.

381 The version of DALEC used in this study is composed of six submodels (i.e.,  
382 photosynthesis, phenology, autotrophic respiration, allocation, litterfall, and decomposition) to  
383 simulate the carbon exchanges among five carbon pools (i.e., leaf, stem, root, soil organic matter  
384 and litter) (Ricciuto et al., 2011). There are 21 parameters in DALEC, of which, 17 parameters  
385 are derived from the six submodels and four parameters serve to initialize the carbon pools.  
386 Table 2 summarizes the names, prior ranges and nominal values of these 21 parameters. The  
387 observation is the Harvard Forest daily net ecosystem exchange (NEE) from year 1992 to 2006.

388 DALEC is coded in Fortran. In windows system, a gfortran compiler converts the model code to  
389 an executable file (i.e., DALEC.exe).

390 Figure 2 is the GUI window of MIDA. We first set up a DA task as described in step 1  
391 using the upper panel. In this application, the number of sampling series is set as 20,000. Once  
392 users click the ‘choose a directory’ or ‘choose a file’ button, a new dialog window will pop up  
393 and users are able to choose the directory or load files interactively. As described in step 1 on  
394 preparation of DA, the working path is where the outputs of DA and ‘ParameterValue.txt’ are  
395 saved (e.g., C:/workingPath). After the output configuration file is loaded, the filenames of  
396 model outputs, observations and their variance will be displayed in the window automatically.  
397 This application only uses a ‘NEE.txt’ observation file. Similarly, after users load parameter  
398 range file (e.g., a file named ‘ParamRange.txt’ contains three rows which are minimum,  
399 maximum and default values of parameters), the content in this file is displayed as well. To  
400 replace the current parameter range file loaded, users can simply upload another file. In this  
401 application, the executive model file is ‘DALEC.exe’ with Fortran compiler in windows system.  
402 Because we do not have parameter covariance information, this input is left blank. After ‘save to  
403 namelist file’ is clicked, a ‘namelist.txt’ file containing all the inputs will be generated in the  
404 working path.

405 After the DA task set up, we load the ‘namelist.txt’ file and click the ‘run data  
406 assimilation’ button in the lower panel to trigger step 2 on execution of DA. A new dialog will  
407 pop up to show the acceptance rate information and notify the termination of DA. Then we will  
408 click the ‘generate plots’ button to visualize the posterior distributions of 21 parameters as  
409 described in step 3.

410       Figure 3 shows that the simulation outputs using the optimized parameter values from  
411    MIDA better fit with the observations than those using default parameter values. Figure 4 depicts  
412    posterior distributions of the 21 parameters estimated from MIDA. More than half of the  
413    parameters are constrained well with a unimodal shape.  $X_{stem_{init}}$  and  $X_{root_{init}}$  have a wide  
414    occupation of the prior range, indicating that the observation data does not provide useful  
415    information for them. The constrained posterior distributions in this study are similar to those  
416    from the study in Lu et al. (2017). Note that MCMC estimates have a large variance and a low  
417    convergence rate especially in high-dimensional problems, with a finite number of samples it is  
418    not expected that two simulations would give exactly the same results.

419  
420    **3.2 Case 2: Application of MIDA to a surrogate land surface model**  
421    This case study is to examine the applicability of MIDA to a surrogate-based land surface model.  
422    The original model is energy exascale earth system model: the land component (ELM) (Ricciuto  
423    et al., 2018). As ELM is computationally expensive (one forward model simulation takes more  
424    than one day), a sparse-grid (SG) surrogate system was developed to reduce the computational  
425    time (Lu et al., 2018). The forcing data for the surrogate model is half-hourly meteorological  
426    measurements at Missouri Ozark flux site from 2006 to 2014. The observations that were used  
427    for optimization are annual sums of net ecosystem exchange (NEE), annual averages of total leaf  
428    area index and latent heat fluxes from 2006 to 2010. The eight parameters selected (Table 3) are  
429    the most important parameters for the variations in outputs (Ricciuto et al., 2018). The model is  
430    written in Python. A ‘pyinstaller’ library packages the model code into an executable file. The  
431    iteration number in MIDA is 20,000.

432       Figure 5 shows posterior distributions of calibrated parameters.  $c_{root}$ ,  $SLA_{top}$ ,  
433     $t_{leaffall}$ ,  $GDD_{onset}$  are constrained well with a unimodal distribution. However, the distribution

434 of the rest 4 parameters (i.e.,  $N_{leaf}$ ,  $CN_{root}$ ,  $A_{r2l}$  and  $Res_m$ ) cluster at near the edge. These  
435 results match well with the study by Lu et al. (2018). As shown in Figure 6, the calibrated  
436 parameters induce a performance improvement in simulating total leaf area index and NEE. For  
437 latent heat, both the default and optimized simulation obtain good agreement with the  
438 observation. These conclusions are also similar to those in Lu et al. (2018).

439 MIDA hides the detailed differences between models. For example, DALEC model in  
440 case 1 is a process-based model to simulate ecosystem carbon cycle while surrogate-based ELM  
441 in case 2 is an approximation of land surface model. They are also different in programming  
442 language, simulation time, forcing data, etc. MIDA is able to deal with models with so many  
443 different characteristics and hides these differences from users. Users only need to indicate the  
444 filenames of the model to be used, its parameter range, the output configuration file, etc. in the  
445 ‘namelist.txt’ file. Thus, MIDA simplified the DA applications using different models.

446

### 447 **3.3 Case 3: Evaluation of multiple phenological models**

448 This study case uses nine phenological models (Yun et al., 2017) to demonstrate the applicability  
449 of MIDA in model comparison. Five out of the nine models predict phenological events, such as  
450 the day of leaf onset, using growing degree days, which are calculated as temperature  
451 accumulation above a base temperature. The other four models consider two processes: chilling  
452 effects of cold temperature on dormancy before budburst and forcing effects of warm  
453 temperature on plant development. Each model uses different response functions to represent  
454 chilling and forcing effects. The detailed model descriptions and associated parameter  
455 information are in supplementary table.

456 Data are from the Spruce and Peatland Responses Under Climatic and Environmental  
457 Change experiment (SPRUCE) (Hanson et al., 2017) located in northern Minnesota, USA. The  
458 experiment consists of five-level whole-ecosystem warming (i.e., +0, +2.25, +4.5, +6.75, +9°C)  
459 and two-level elevated  $CO_2$  concentrations (i.e., +0, +500ppm). Dates of leaf onset were  
460 observed with PhenoCam (Richardson et al., 2018) for tree species: *Picea mariana* and *Larix*  
461 *laricina*. For the sake of demonstration of MIDA application, we only show DA results for *Larix*  
462 *laricina* with +9°C warming treatment and +0 ppm  $CO_2$  treatment from 2016 to 2018.

463 MIDA was used to compare performances of the nine models in reference to the same  
464 observations of leaf onset dates after DA. We as users changed filenames of model executable  
465 file (i.e., PhenoModels.exe), defined parameter ranges, and assigned the directory of working  
466 path for each model. MIDA then estimated the optimized parameters and save the corresponding  
467 best simulation outputs to the working path for each of the nine models. Figure 7 shows the best  
468 simulation output of these nine models. The simulation output of the 6<sup>th</sup>, 7<sup>th</sup>, 8<sup>th</sup>, and 9<sup>th</sup> models  
469 better fit the observation than the other models. It demonstrates that models that consider both  
470 chilling and heating effects can achieve good simulations of the leaf onset dates.

471

472 **3.4 Case 4: Supporting data assimilation with a dynamic vegetation model**

473 This case study is to examine the efficiency of MIDA to integrate remote sensing data into a  
474 dynamic vegetation model. The model used in this study is Biome Ecological strategy simulator  
475 (BiomeE) (Weng et al., 2019). This model simulates vegetation demographic processes with  
476 individual-based competition for light, soil water, and nutrients. Individual trees in BiomeE  
477 model are represented by cohorts of trees with similar sizes. The light competition among  
478 cohorts is based on their heights and crown areas according to the rule of perfect plasticity

479 approximation (PPA) model (Strigul et al., 2008). Each cohort has seven pools: leaves, roots,  
480 sapwood, heartwood, seeds, nonstructural carbon and nitrogen. After carbon are assimilated into  
481 plants via photosynthesis, the assimilated carbon enters to nonstructural carbon pool and is used  
482 for plant growth (i.e., diameter, height, crown area) and reproduction according to empirical  
483 allometric equations (Weng et al., 2019). In this application, two parameters to be constrained  
484 (Table 4) are annual productivity rate and annual mortality rate of trees.

485 Observations to be used in DA are leaf area indexes in six vertical heights (i.e., 0-5m, 6-  
486 10m, 11-15m, 16-20m, 21-25m, and 26-30m) at Willow Creek study site, Wisconsin, USA. The  
487 forest at the site is an upland deciduous broadleaf forest of around 302 years old. The  
488 observations were from Global Ecosystem Dynamics Investigation (GEDI) acquired by a Light  
489 Detection and Ranging (Lidar) laser system, which is deployed on the International Space  
490 Station (ISS) by NASA in 2018 (Dubayah et al., 2020). The observations were first averaged  
491 from three footprints and then leaf area indexes in the six canopy layers were standardized to be  
492 summed up as one.

493 To use MIDA, we reorganized the simulation outputs to match observations as suggested  
494 in section 2.6. The BiomeE model simulates leaf areas in eight layers (i.e., 0-5m, 6-10m, 11-  
495 15m, 16-20m, 21-25m, 26-30m, 31-35m, and 36-40m) from 0 to 800 years. An output  
496 configuration file was provided to post-process model outputs of leaf area indexes in six layers to  
497 match observations at the forest age of 302 years. These simulated leaf area indexes in the six  
498 canopy layers were also standardized to match standardized observations of leaf area indexes.  
499 The observations and post-processed simulation outputs were saved to ‘LAI.txt’ and  
500 ‘simu\_LAI.txt’ files, respectively. The two files are used in MIDA for data assimilation to  
501 generate posterior distributions of estimated two parameters as showed in figure 8. The

502 optimized parameter values through maximum likelihood estimation are different from their  
503 default values. Figure 9 compares the simulation outputs with optimized parameters estimated by  
504 MIDA to those with default parameter values. After DA with GEDI data in MIDA, the  
505 simulation accuracy of leaf area index is substantially improved especially in middle (16~20m)  
506 and highest (26~30m) layers.

507

#### 508 **4. Discussion**

509 This study introduced MIDA as a model-independent tool to facilitate the applications of data  
510 assimilation in ecology and biogeochemistry. The potential user community is ecologists with  
511 limited knowledge of model programming and technical implementation of DA algorithms.  
512 Several model-independent DA tools have already been developed, such as DART (Anderson et  
513 al., 2009), openDA (Ridler et al., 2014), PDAF (Nerger and Hiller, 2013) and PEST (Doherty,  
514 2004), mainly for applications in research areas of hydrology, atmosphere, and remote sensing.  
515 These DA tools either use gradient descent method, such as Levenburg-Marquardt algorithm in  
516 PEST, or Kalman Filter methods, such as EnKF in DART, openDA, and PDAF. The Levenburg-  
517 Marquardt algorithm is a local search method, which is hard to find global optimization solution  
518 for highly nonlinear models. EnKF updates state variables and parameter values each time when  
519 observations are sequentially assimilated, resulting discrete values of estimated parameters.  
520 Jumps in estimated parameter values by EnKF make it very difficult to obey mass conservation  
521 in biogeochemical models (Gao et al., 2011). In this study, we used the MCMC method in MIDA  
522 to generate parameter values and their posterior distributions. MCMC is a widely used method in  
523 many DA studies with biogeochemical models but has been applied to individual models with  
524 invasive coding (Bloom et al., 2016; Hararuk et al., 2015; Liang et al., 2018; Luo and Schuur,

525 2020; Ricciuto et al., 2011). Compared to the other model-independent DA tools mentioned  
526 above, MIDA is the first tool that uses the MCMC method for DA.

527 Biogeochemical models are incorporating more detailed processes related to carbon and  
528 nitrogen cycles (Lawrence et al. 2020). Complex biogeochemical models yield predictions with  
529 great uncertainty (Frielingstein et al. 2009 and 2014). Data assimilation has been increasingly  
530 used to estimate parameter values against observations and reduce uncertainty in model  
531 prediction (Luo et al. 2016, Luo and Schuur 2020). However, current applications of DA are  
532 almost all model dependent. It requires ecologists to write code to integrate DA algorithm with  
533 models. The coding practice is a big technical challenge for ecologists with limited program  
534 ability. The distinct advantage of MIDA is to enable ecologists to conduct model independent  
535 DA. MIDA streamlines workflow of the three-step procedure for DA to enable users to conduct  
536 DA without extensive coding. Users mainly need to provide numerical and character values for  
537 data exchanges to transfer data (i.e., parameter values, simulation outputs, observations) between  
538 the model and MIDA by a file named ‘namelist.txt’ or by interactive inputs via a GUI window  
539 (Fig. 2).

540 We tested MIDA in four cases for its applicability to ecological models. The first case is  
541 applied to DALEC model, which has been used in several data assimilation studies (Bloom et al.,  
542 2016; Lu et al., 2017; Safta et al., 2015; Williams et al., 2005). The previous DA studies all used  
543 invasive coding to incorporate DA algorithm into models. As demonstrated in this study, MIDA  
544 was applied to DALEC without invasive coding but by providing the directory to save DA  
545 results and filenames of DALEC model executable, parameter prior range, and output  
546 configuration file through the ‘namelist.txt’ file or interactive inputs in the first preparation step  
547 of the workflow. Then, MIDA run DA as a black box with DALEC before visualizing the DA

548 results. Next, we tested the applicability of MIDA a surrogate-based ELM model and a dynamic  
549 vegetation model BiomeE. To switch the test case from DALEC to the surrogate-based ELM  
550 model and the BiomeE model, we changed the filenames of model executable, parameter prior  
551 range, and output configuration file in the ‘namelist.txt’ file for MIDA. This flexibility of MIDA  
552 in switching models for DA makes it much easier for model comparisons. We tested this  
553 capability of MIDA with nine phenological models to compare alternative model structures.  
554 Similarly, MIDA enables efficient switches of observations to be assimilated into models. Users  
555 only need to change filenames of observations in the output configuration file. This feature of  
556 MIDA makes it easier to utilize abundant traits databases such as TRY (Kattge et al., 2020),  
557 FRED (Iversen et al., 2017), etc. Moreover, this feature of MIDA also helps evaluating the  
558 relative information content of different observations for constraining model parameters and  
559 prediction (Weng and Luo, 2011). Consequently, MIDA can facilitate selection of the most  
560 informative observations and then better guide data collections in filed experiments. Ultimately,  
561 MIDA can aid ecological forecasting and help reduce uncertainty in model predictions (Huang et  
562 al., 2018; Jiang et al., 2018).

563         Although MIDA helps users to get rid of model detail, users may still need basic  
564 knowledge about the model outputs to prepare the output configuration file which is to match  
565 model outputs to observations one-by-one (see Section 2.6). This effort of preparing the  
566 correspondence between model outputs and observations for MIDA is not that difficult because  
567 users are reading or writing a text file and most model developers will provide reference to help  
568 understanding observations or model output files.

569         Generally, MIDA requires longer time to run DA than the embedded DA algorithm,  
570 because MIDA calls model simulation as an external executable rather than a function

571 embedded. Thus, we recommend MIDA for beginners of DA users with models that are less  
572 complex. Besides, the current version of MIDA only incorporates Metropolis-Hasting sampling  
573 approach. More MCMC methods (e.g., Hamiltonian Monte Carlo) may be incorporated into  
574 MIDA in the future.

575

## 576 **5. Conclusions**

577 We developed MIDA to facilitate data assimilation for biogeochemical models. Traditional DA  
578 studies require ecologists to program codes to integrate DA algorithms into model source codes.  
579 The easy-to-use MIDA module enables ecologists to conduct model-independent DA without  
580 extensive coding thus advancing the application of DA for ecological modeling and forecasting.  
581 We demonstrated the capability of MIDA in four cases with a total of 12 ecological models.  
582 These cases showed that MIDA is easy to perform for a variety of models and can efficiently  
583 produce accurate parameter posterior distributions. Moreover, MIDA supports flexible usage of  
584 different models and different observations in the DA analysis and allows a quick switch from  
585 one model to another. This capability enables MIDA to serve as an efficient tool for model  
586 intercomparison projects and enhancing ecological forecasting.

587

## 588 **Appendix A:** Nine phenological models

### 589 1. Growing degree (GD)

590 The growing degree (GD) model is one of the most widespread phenological model to simulate  
591 the date of leaf onset ( $\widehat{D}$ ). In this study, the time scale is limited to daily based on observation  
592 records. The kernel of GD is to calculate the growing degree days (GDD,  $\sum_{d=D_s}^{\widehat{D}-1} \Delta d$ ) which is the  
593 heat accumulation above a base temperature ( $T_b$ ). For simplicity, the daily temperature ( $T_d$ ) can

594 be approximated by the average of daily maximum and minimum temperatures. The heat  
 595 accumulation starts at day  $D_s$ , which is empirically estimated, and ends when GDD reaches a  
 596 forcing requirement threshold ( $R_d$ ). Two parameters to be constrained are base temperature ( $T_b$ )  
 597 and the forcing requirement ( $R_d$ ). Their default values and prior range are listed in Table A1.

598 
$$\Delta d = \begin{cases} T_d - T_b & \text{if } T_d > T_b \\ 0 & \text{otherwise} \end{cases} \quad (\text{A1})$$

599 
$$\sum_{d=D_s}^{\hat{D}-1} \Delta d < R_d \leq \sum_{d=D_s}^{\hat{D}} \Delta d \quad (\text{A2})$$

600 2. Sigmoid function (SF)

601 Compared to the linear response function of GDD in GD model, the sigmoid function (SF)  
 602 model provides a non-linear function to better represent the non-linearity of the growth response  
 603 to heat accumulation. Three parameters to be constrained in DA are base temperature ( $T_b$ ), the  
 604 forcing requirement ( $R_d$ ) and temperature sensitivity ( $S_t$ ). Their default values and prior range  
 605 are listed in Table A1.

606 
$$\Delta d = \frac{1}{1+e^{S_t(T_d-T_b)}} \quad (\text{A3})$$

607 
$$\sum_{d=D_s}^{\hat{D}-1} \Delta d < R_d \leq \sum_{d=D_s}^{\hat{D}} \Delta d \quad (\text{A4})$$

608 3. Beta function (BF)

609 In reality, the plant growth rate, as described with  $\Delta d$ , gradually increases up to a specific  
 610 temperature, then rapidly declines to a supra-optimal level. Such response can be well described  
 611 by a beta function with uni-modality and non-symmetrical shape. Three parameters are involved  
 612 in DA: minimum temperature ( $T_n$ ), optimal temperature ( $T_o$ ) and forcing requirement ( $R_d$ ). The  
 613 other parameter values are fixed with empirical values. For example, maximum growth rate ( $R_x$ )  
 614 is set to one and maximum temperature ( $T_x$ ) is assumed to be 45.

615 
$$r_d = R_x \left( \frac{T_x - T_d}{T_x - T_o} \right) \left( \frac{T_d - T_n}{T_o - T_n} \right)^{\frac{T_o - T_n}{T_x - T_o}} \quad (\text{A5})$$

616 
$$\Delta d = \begin{cases} r_d & \text{if } r_d > 0 \\ 0 & \text{otherwise} \end{cases} \quad (\text{A6})$$

617 
$$\sum_{d=D_s}^{\widehat{D}-1} \Delta d < R_d \leq \sum_{d=D_s}^{\widehat{D}} \Delta d \quad (\text{A7})$$

618 4. Days transferred to standard temperature (DTS)

619 According to Arrhenius las, the relationship between growth rate and daily temperature  $T_d$  can  
 620 be interpolated by the equation 8 (Ono and Konno, 1999). With a factor weighted by standard  
 621 temperature, the equation for DTS (Eq. A9) can better represent growth rate dependent on  
 622 temperatures. Three parameters considered in DA are: temperature sensitivity rate ( $E_a$ ), standard  
 623 temperature ( $T_s$ ) and forcing requirement ( $R_d$ ).

624 
$$k = e^{\frac{-E_a}{R \cdot T_d}} \quad (\text{A8})$$

625 
$$\Delta d = e^{\frac{E_a(T_d - T_s)}{R \cdot T_d \cdot T_s}} \quad (\text{A9})$$

626 
$$\sum_{d=D_s}^{\widehat{D}-1} \Delta d < R_d \leq \sum_{d=D_s}^{\widehat{D}} \Delta d \quad (\text{A10})$$

627 5. Thermal period fixed model (TP)

628 The difference between GD and TP models are heat accumulation occurs in a fixed time period  
 629 ( $D_n$ ). The day of leaf onset is the last day ( $\widehat{D}_s + D_n$ ) when the accumulated heat reaches the  
 630 forcing requirement. The start day ( $\widehat{D}_s$ ) of heat accumulation begins in day one and moves one  
 631 day forward each time to estimate Eq. (A12). Three parameters are involved in DA: the base  
 632 temperature ( $T_b$ ), the period length ( $D_n$ ) and the forcing requirement ( $R_d$ ).

633 
$$\Delta d = \begin{cases} T_d - T_b & \text{if } T_d > T_b \\ 0 & \text{otherwise} \end{cases} \quad (\text{A11})$$

634 
$$R_d \leq \sum_{d=\widehat{D}_s}^{\widehat{D}_s+D_n} \Delta d \quad (\text{A12})$$

635 6. Chilling and forcing (CF)

636 Compared to GD, there is another distinctive chilling period for dormancy. CF model  
 637 sequentially calculates two accumulations in opposite directions: chilling accumulation and anti-  
 638 chilling accumulation. The start day of chilling accumulation ( $D_s$ ) is implicitly set as 273.0  
 639 which is October 1<sup>st</sup>. The end day of chilling accumulation ( $D_0$ ) is the beginning of anti-chilling  
 640 accumulation. Three parameters are considered in DA: the chilling requirement ( $R_d^C$ ) and the  
 641 forcing requirement ( $R_d^F$ ), the temperature threshold ( $T_c$ ).

$$642 \quad \Delta_d = \begin{cases} T_d - T_c & \text{if } T_d \geq 0 \\ -T_c & \text{otherwise} \end{cases} \quad (\text{A13})$$

$$643 \quad \Delta_d^C = \begin{cases} \Delta_d & \text{if } \Delta_d < 0 \\ 0 & \text{otherwise} \end{cases} \quad (\text{A14})$$

$$644 \quad \Delta_d^F = \begin{cases} \Delta_d & \text{if } \Delta_d > 0 \\ 0 & \text{otherwise} \end{cases} \quad (\text{A15})$$

$$645 \quad \sum_{d=D_s}^{D_0-1} \Delta_d^C > R_d^C \geq \sum_{d=D_s}^{D_0} \Delta_d^C \quad (\text{A16})$$

$$646 \quad \sum_{d=D_0}^{\widehat{D}-1} \Delta_d^F < R_d^F \leq \sum_{d=D_0}^{\widehat{D}} \Delta_d^F \quad (\text{A17})$$

## 647 7. Sequential model (SM)

648 The difference between CF and SM models is that SM used a beta function (Eq. A18) for the  
 649 calculation of chilling accumulation and adopted a sigmoid function (Eq. A20) for anti-chilling  
 650 accumulation. The detailed descriptions of these two functions can be referred to the  
 651 introductions of BF model and CF model. The maximum temperature is empirically set as  
 652 13.7695. Six parameters are constrained in DA: minimum temperature ( $T_n$ ), optimal temperature  
 653 ( $T_o$ ), temperature sensitivity ( $S_t$ ), forcing base temperature ( $T_b$ ), chilling requirement ( $R_d^C$ ), and  
 654 forcing requirement ( $R_d^F$ ).

$$655 \quad r_d = \left( \frac{T_x - T_d}{T_x - T_o} \right) \left( \frac{T_d - T_n}{T_o - T_n} \right)^{\frac{T_o - T_n}{T_x - T_o}} \quad (\text{A18})$$

$$656 \quad \Delta_d^C = \begin{cases} r_d & \text{if } r_d < 0 \\ 0 & \text{otherwise} \end{cases} \quad (\text{A19})$$

657 
$$\Delta_d^F = \frac{1}{1+e^{S_t(T_d-T_b)}}$$
 (A20)

658 
$$\sum_{d=D_s}^{D_0-1} \Delta_d^C > R_d^C \geq \sum_{d=D_s}^{D_0} \Delta_d^C$$
 (A21)

659 
$$\sum_{d=D_0}^{\widehat{D}-1} \Delta_d^F < R_d^F \leq \sum_{d=D_0}^{\widehat{D}} \Delta_d^F$$
 (A22)

660 8. Parallel model (PM)

661 Critical difference between PM and above two-step models is that the chilling and anti-chilling  
 662 accumulations happen simultaneously (Fu et al., 2012). In the earlier dates during chilling  
 663 period, only small fraction ( $K_d$ ) of forcing (Eq. A25) will be accumulated. The maximum  
 664 temperature is empirically set as 15.3. Seven parameters will be considered in DA: minimum  
 665 temperature ( $T_n$ ), optimal temperature ( $T_o$ ), temperature sensitivity ( $S_t$ ), forcing base temperature  
 666 ( $T_b$ ), chilling requirement ( $R_d^C$ ), forcing requirement ( $R_d^F$ ), and a forcing weight coefficient ( $K_m$ ).

667 
$$r_d = \left( \frac{T_x - T_d}{T_x - T_o} \right) \left( \frac{T_d - T_n}{T_o - T_n} \right)^{\frac{T_o - T_n}{T_x - T_o}}$$
 (A23)

668 
$$\Delta_d^C = \begin{cases} r_d & \text{if } r_d < 0 \\ 0 & \text{otherwise} \end{cases}$$
 (A24)

669 
$$K_d = \begin{cases} K_m + (1 - K_m) \frac{\sum_{i=D_s}^d \Delta_i^C}{R_d^C} & \text{if } \sum_{d=D_s}^{D_0-1} \Delta_d^C > R_d^C \\ 1 & \text{otherwise} \end{cases}$$
 (A25)

670 
$$\Delta_d^F = \frac{K_d}{1+e^{S_t(T_d-T_b)}}$$
 (A26)

671 
$$\sum_{d=D_s}^{D_0-1} \Delta_d^C > R_d^C \geq \sum_{d=D_s}^{D_0} \Delta_d^C$$
 (A27)

672 
$$\sum_{d=D_0}^{\widehat{D}-1} \Delta_d^F < R_d^F \leq \sum_{d=D_0}^{\widehat{D}} \Delta_d^F$$
 (A28)

673 9. Alternating model (AM)

674 AM fixes the start date of chilling period ( $D_s^C$ ) as November 1<sup>st</sup> and the start date of anti-chilling  
 675 period ( $D_s^F$ ) as January 1<sup>st</sup>. The difference between AM and the other models above is that the  
 676 forcing requirement is not a parameter value but is decided by the length of chilling days (Fu et

677 al., 2012). Five parameters to be constrained in DA are: chilling temperature ( $T_c$ ), forcing base  
 678 temperature ( $T_b$ ) and three coefficients ( $a, b, c$ ) in calculation of forcing requirement.

679 
$$\Delta_d^C = \begin{cases} 1 & \text{if } T_d \leq T_c \\ 0 & \text{otherwise} \end{cases} \quad (\text{A29})$$

680 
$$\Delta_d^F = \begin{cases} T_d - T_b & \text{if } T_d > T_b \\ 0 & \text{otherwise} \end{cases} \quad (\text{A30})$$

681 
$$R_d^C = \sum_{i=D_s^C}^d \Delta_i^C \quad (\text{A31})$$

682 
$$R_d^F = a + b \cdot e^{-c \cdot R_d^C} \quad (\text{A32})$$

683 
$$\sum_{d=D_s^F}^{\widehat{D}-1} \Delta_d^F < R_d^F \leq \sum_{d=D_s^F}^{\widehat{D}} \Delta_d^F \quad (\text{A33})$$

684

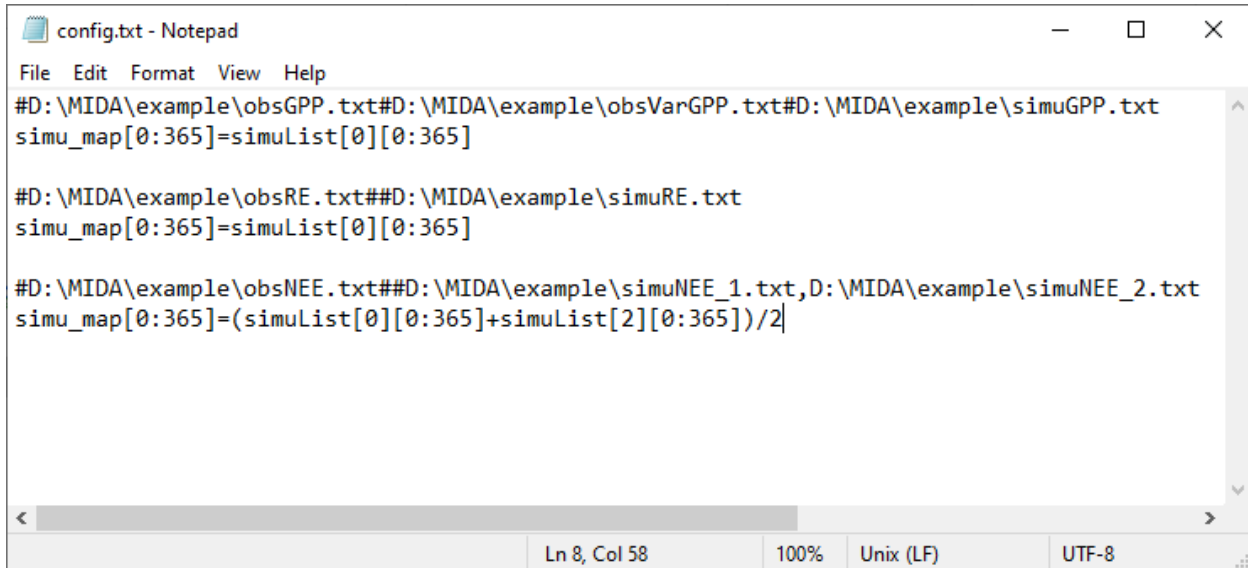
685 Table A1: A summary of parameters to be calibrated in nine phenological models. Their default  
 686 parameter value and prior parameter range are shown.

Model	Parameter	Description	Unit	Default	Range
GD	$T_b$	Base temperature	°C	10	[-5, 25]
	$R_d$	Forcing requirement	°Cd	35	[0, 200]
SF	$T_b$	Base temperature	°C	-1.5	[-10, 25]
	$R_d$	Forcing requirement	°C	50	[0, 500]
BF	$T_o$	Optimal temperature	°C	15	[10, 35]
	$T_n$	Minimum temperature	°C	0	[-10, 5]
	$R_d$	Forcing requirement	°Cd	11	[0, 50]
DTS	$E_a$	Temperature sensitivity rate	-	250	[1, 1500]
	$T_s$	Standard temperature	°C	10	[-30, 40]
	$R_d$	Forcing requirement	°Cd	50	[1, 200]
TP	$T_b$	Base temperature	°C	12.5	[0, 30]
	$D_n$	Period length	d	25	[0, 50]
	$R_d$	Forcing requirement	°Cd	20	[0, 150]
CF	$R_d^C$	Chilling requirement	°Cd	-124	[-300, 0]
	$R_d^F$	Forcing requirement	°Cd	120	[0, 300]
	$T_c$	Chilling base temperature	°C	5	[0, 30]
SM	$T_n$	Minimum temperature	°C	-20	[-80, 0]
	$T_o$	Optimal temperature	°C	0	[-26, 10]
	$S_t$	Temperature sensitivity	-	-1.8	[-5, 0]
	$T_b$	Forcing base temperature	°C	5	[-5, 35]
	$R_d^C$	Chilling requirement	°Cd	20	[0, 80]
	$R_d^F$	Forcing requirement	°Cd	20	[0, 80]
PM	$T_n$	Minimum temperature	°C	-20	[-80, 0]
	$T_o$	Optimal temperature	°C	0	[-26, 10]
	$S_t$	Temperature sensitivity	-	-0.6	[-1, 0]
	$T_b$	Forcing base temperature	°C	5	[-5, 35]
	$R_d^C$	Chilling requirement	°Cd	11.35	[0, 80]
	$R_d^F$	Forcing requirement	°Cd	44.01	[0, 80]
AM	$K_m$	Forcing weight coefficient	-	0.2	[0, 1]
	$T_c$	Chilling base temperature	°C	4.6	[-10, 10]
	$T_b$	Forcing base temperature	°C	5	[-5, 35]
	a	Coefficient for forcing adjustment	-	11.51	[0.01, 15]
	b	Coefficient for forcing adjustment	-	88	[0, 200]
	c	Coefficient for forcing adjustment	-	-0.01	[-1, -10 <sup>-4</sup> ]

687

688

689 **Appendix B:** An example of output configuration file  
690 Output configuration file (e.g., config.txt) is to indicate the directories of observations and  
691 simulation output files as well as how they map to each other. Figure B1 is an example of the  
692 output configuration file. There are three blocks of functions to map simulation outputs to  
693 observed GPP, RE, and NEE. The blocks of mapping functions are separated by a blank line.  
694 Each mapping block starts with the directories of one observation, its observation variance and  
695 model outputs, which are separated by a hash key. If there is no observation variance available,  
696 users can ignore this directory. If multiple simulation outputs are used to correspond to one  
697 observation, the directories of simulation outputs are separated by a comma. The rest of the  
698 mapping block describes how to map simulation outputs to observations. The simu\_map variable  
699 is simulation output after mapping. The simuList variable saves the simulation outputs specified  
700 in the first line. Taking the third mapping block in Fig. B1 as an example, simuList[0] saves  
701 contents in simuNEE\_1.txt and simuList[0][0:365] saves the first 365 elements in this file.



```
config.txt - Notepad
File Edit Format View Help
#D:\MIDA\example\obsGPP.txt#D:\MIDA\example\obsVarGPP.txt#D:\MIDA\example\simuGPP.txt
simu_map[0:365]=simuList[0][0:365]

#D:\MIDA\example\obsRE.txt##D:\MIDA\example\simuRE.txt
simu_map[0:365]=simuList[0][0:365]

#D:\MIDA\example\obsNEE.txt##D:\MIDA\example\simuNEE_1.txt,D:\MIDA\example\simuNEE_2.txt
simu_map[0:365]=(simuList[0][0:365]+simuList[2][0:365])/2
```

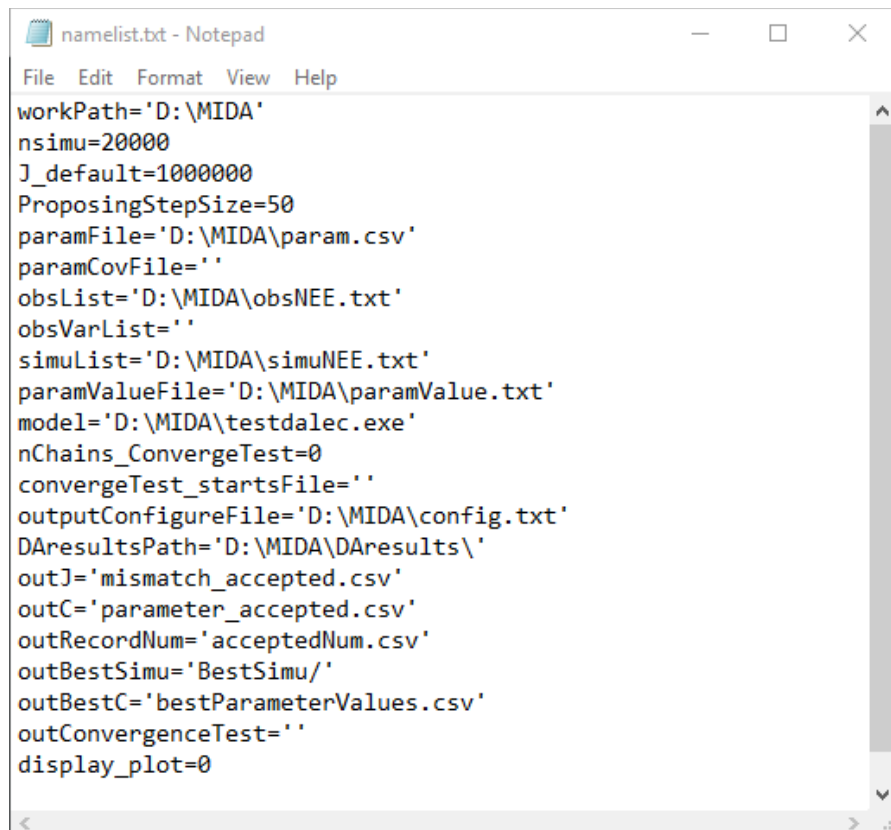
702  
703 Figure B1: An example of output configuration file

704 **Appendix C:** An example of the namelist.txt file  
705 The Fig. C1 shows an example of the namelist.txt for the first study case with the DALEC  
706 model. Users need to prepare the namelist.txt before execution of data assimilation (DA) either  
707 manually or via GUI. Below describes the content in the namelist.txt. Detailed explanation or  
708 tutorials are available in the Zenodo repositories at the end of the appendixes.

709 ‘workpath’ is the directory where the MIDA executable are saved. ‘nsimu’ is the number  
710 of iterations in execution of data assimilation. ‘J\_default’ is the default mismatch (i.e., cost  
711 function) to be compared in the first moving phase of data assimilation. ‘ProposingStepSize’  
712 controls the jump scale in the proposing phase of data assimilation. Users can increase or  
713 decrease this value to adjust the acceptance rate to be in a range from 0.2 to 0.5. ‘paramFile’ is  
714 the directory of a csv file saving parameter-related information such as parameter range.  
715 ‘obsList’ saves the directories of observations. Multiple observations are separated by semicolon.  
716 Similarly, ‘obsVarList’ saves the directories of observation variance in the same order as that of  
717 ‘obsList’. ‘simuList’ saves the directories of simulation outputs corresponding to the  
718 observations. With GUI, MIDA reads directories in the output configuration file (e.g., config.txt)  
719 which users provide and assign values for ‘obsList’, ‘obsVarList’, and ‘simuList’ in the  
720 namelist.txt automatically. In this case, if the directories of observations change, users only need  
721 to modify the output configuration file and generate the namelist.txt again with GUI-based  
722 MIDA.

723 ‘paramValue’ is the directory of a txt file where MIDA writes out new set of parameter  
724 values for model execution in each iteration of data assimilation. Its default value is  
725 ‘ParameterValue.txt’ under the workpath specified in the first line of the namelist.txt. ‘model’  
726 saves the directory of model executable. ‘nChains\_convergeTest’ indicates whether to conduct

727 German-Rubin (G-R) convergence test or not. If G-R test is used, its values is the number of  
 728 multiple MCMC chains. If not, its value is zero. ‘convergeTest\_startsFile’ is the directory of a  
 729 csv file saving default parameter values as the start points in multiple MCMC chains.  
 730 ‘outConvergenceTest’ saves the results of G-R test. If ‘nChains\_ConvergeTest’ is zero, both  
 731 values of ‘convergeTest\_startsFile’ and ‘outConvergenceTest’ are empty. ‘DAresultsPath’ is the  
 732 directory saving the results of DA whose directories are also listed in the following six lines:  
 733 ‘outJ’ for the accepted mismatches; ‘outC’ for the accepted parameter values; ‘outRecordNum’  
 734 for the number of accepted parameter values; ‘outBestSimu’ for the best simulation outputs with  
 735 the optimal parameter values; ‘outBestC’ for the optimal parameter values. For MIDA without  
 736 GUI, ‘display\_plot’ indicates whether or not to visualize the posterior distributions after DA.



```

namelist.txt - Notepad
File Edit Format View Help
workPath='D:\MIDA'
nsimu=20000
J_default=1000000
ProposingStepSize=50
paramFile='D:\MIDA\param.csv'
paramCovFile=''
obsList='D:\MIDA\obsNEE.txt'
obsVarList=''
simulist='D:\MIDA\simuNEE.txt'
paramValueFile='D:\MIDA\paramValue.txt'
model='D:\MIDA\testdalec.exe'
nChains_ConvergeTest=0
convergeTest_startsFile=''
outputConfigureFile='D:\MIDA\config.txt'
DAresultsPath='D:\MIDA\DAresults\
outJ='mismatch_accepted.csv'
outC='parameter_accepted.csv'
outRecordNum='acceptedNum.csv'
outBestSimu='BestSimu/'
outBestC='bestParameterValues.csv'
outConvergenceTest=''
display_plot=0
  
```

737  
 738 **Figure C1.** An example of the ‘namelist.txt’ file. In order to use MIDA, users need to prepare  
 739 data and a model and specify their file names and directories in the ‘namelist.txt’ file.

740 *Code and data availability.* The code of MIDA is available at the Zenodo repository  
741 <https://doi.org/10.5281/zenodo.4762725> (last access: May 2021). Data used in this study are  
742 available at <https://doi.org/10.5281/zenodo.4762779>. A comparison of the time cost using the  
743 embedded DA algorithm and MIDA is available at the Zenodo repository  
744 <https://doi.org/10.5281/zenodo.4891319>.

745

746 *Video supplement.* Tutorial videos of how to use MIDA is available at  
747 <https://doi.org/10.5281/zenodo.4762777>

748

749 *Author contributions.* XH, IS, and YL designed the study. XH built the workflow of MIDA and  
750 tested its capability in four cases. DL, DMR, and PJH provided data and model for the first and  
751 second test cases. XL prepared models and ADR provided observations for the third case. EW  
752 and SN helped to prepare data and model for the fourth case. XH, LJ, EH and YL analyzed the  
753 results. All authors contributed to the preparation of the manuscript.

754

755 *Competing interests.* The authors declare that they have no conflict of interest.

756

757 *Acknowledgements.* This work was funded by subcontract 4000158404 from Oak Ridge National  
758 Laboratory (ORNL) to the Northern Arizona University. ORNL is managed by UT-Battelle,  
759 LLC, for the U.S. Department of Energy under contract DE-AC05-00OR22725. EW is supported  
760 by NASA Modeling, Analysis, and Prediction Program (NNH16ZDA001N-MAP)

761

762

763    **References**

764 Allen, J. I., Eknes, M. and Evensen, G.: An Ensemble Kalman Filter with a complex marine  
765 ecosystem model: hindcasting phytoplankton in the Cretan Sea, *Ann. Geophys.*, 21(1), 399–411,  
766 doi:10.5194/angeo-21-399-2003, 2003.

767 Anderson, J., Hoar, T., Raeder, K., Liu, H., Collins, N., Torn, R. and Avellano, A.: The data  
768 assimilation research testbed a community facility, *Bull. Am. Meteorol. Soc.*, 90(9), 1283–1296,  
769 doi:10.1175/2009BAMS2618.1, 2009.

770 Bloom, A. A., Exbrayat, J. F., Van Der Velde, I. R., Feng, L. and Williams, M.: The decadal state of  
771 the terrestrial carbon cycle: Global retrievals of terrestrial carbon allocation, pools, and residence  
772 times, *Proc. Natl. Acad. Sci.*, 113(5), 1285–1290, doi:10.1073/pnas.1515160113, 2016.

773 Bonan, G.: *Climate Change and Terrestrial Ecosystem Modeling*, Cambridge University Press.,  
774 2019.

775 Box, G. E. P. and Tiao, G. C.: *Bayesian Inference in Statistical Analysis*, John Wiley & Sons, Inc.,  
776 Hoboken, NJ, USA., 1992.

777 Ciais, P., Chris, S., Govindasamy, B., Bopp, L., Brovkin, V., Canadell, J., Chhabra, A., Defries, R.,  
778 Galloway, J. and Heimann, M.: Carbon and other biogeochemical cycles, *Clim. Chang.* 2013  
779 *Phys. Sci. Basis*, 465–570, 2013.

780 Cline, M. P., Lomow, G. and Girou, M.: *C++ FAQs*, Pearson Education., 1998.

781 Doherty, J.: *PEST: Model independent parameter estimation*. Fifth edition of user manual,  
782 Watermark Numer. Comput., doi:10.1016/B978-0-08-098288-5.00031-2, 2004.

783 Evensen, G.: The Ensemble Kalman Filter: Theoretical formulation and practical implementation,  
784 *Ocean Dyn.*, 53(4), 343–367, doi:10.1007/s10236-003-0036-9, 2003.

785 Fer, I., Kelly, R., Moorcroft, P. R., Richardson, A. D., Cowdery, E. M. and Dietze, M. C.: Linking

786 big models to big data: Efficient ecosystem model calibration through Bayesian model  
787 emulation, *Biogeosciences*, 15(19), 5801–5830, doi:10.5194/bg-15-5801-2018, 2018.

788 Fox, A., Williams, M., Richardson, A. D., Cameron, D., Gove, J. H., Quaife, T., Ricciuto, D.,  
789 Reichstein, M., Tomelleri, E., Trudinger, C. M. and Van Wijk, M. T.: The REFLEX project:  
790 Comparing different algorithms and implementations for the inversion of a terrestrial ecosystem  
791 model against eddy covariance data, *Agric. For. Meteorol.*, 149(10), 1597–1615,  
792 doi:10.1016/j.agrformet.2009.05.002, 2009.

793 Fox, A. M., Hoar, T. J., Anderson, J. L., Arellano, A. F., Smith, W. K., Litvak, M. E., MacBean, N.,  
794 Schimel, D. S. and Moore, D. J. P.: Evaluation of a Data Assimilation System for Land Surface  
795 Models Using CLM4.5, *J. Adv. Model. Earth Syst.*, 10(10), 2471–2494,  
796 doi:10.1029/2018MS001362, 2018.

797 Friedlingstein, P., Cox, P., Betts, R., Bopp, L., von Bloh, W., Brovkin, V., Cadule, P., Doney, S.,  
798 Eby, M., Fung, I., Bala, G., John, J., Jones, C., Joos, F., Kato, T., Kawamiya, M., Knorr, W.,  
799 Lindsay, K., Matthews, H. D., Raddatz, T., Rayner, P., Reick, C., Roeckner, E., Schnitzler, K.-  
800 G., Schnur, R., Strassmann, K., Weaver, A. J., Yoshikawa, C. and Zeng, N.: Climate–Carbon  
801 Cycle Feedback Analysis: Results from the C4MIP Model Intercomparison, *J. Clim.*, 19(14),  
802 3337–3353, doi:10.1175/JCLI3800.1, 2006.

803 Fu, Y. H., Campioli, M., Van Oijen, M., Deckmyn, G. and Janssens, I. A.: Bayesian comparison of  
804 six different temperature-based budburst models for four temperate tree species, *Ecol. Modell.*,  
805 230, 92–100, doi:10.1016/j.ecolmodel.2012.01.010, 2012.

806 Gao, C., Wang, H., Weng, E., Lakshmivarahan, S., Zhang, Y. and Luo, Y.: Assimilation of multiple  
807 data sets with the ensemble Kalman filter to improve forecasts of forest carbon dynamics, *Ecol.*  
808 *Appl.*, 21(5), 1461–1473, doi:10.1890/09-1234.1, 2011.

809 Gelman, A. and Rubin, D. B.: Inference from Iterative Simulation Using Multiple Sequences, Stat.  
810 Sci., 7(4), 457–472, doi:10.1214/SS/1177011136, 1992.

811 Hanson, P. J., Riggs, J. S., Nettles, W. R., Phillips, J. R., Krassovski, M. B., Hook, L. A., Gu, L.,  
812 Richardson, A. D., Aubrecht, D. M., Ricciuto, D. M., Warren, J. M. and Barbier, C.: Attaining  
813 whole-ecosystem warming using air and deep-soil heating methods with an elevated CO<sub>2</sub>  
814 atmosphere, Biogeosciences, 14(4), 861–883, doi:10.5194/bg-14-861-2017, 2017.

815 Hararuk, O., Xia, J. and Luo, Y.: Evaluation and improvement of a global land model against soil  
816 carbon data using a Bayesian Markov chain Monte Carlo method, J. Geophys. Res.  
817 Biogeosciences, 119(3), 403–417, doi:10.1002/2013JG002535, 2014.

818 Hararuk, O., Smith, M. J. and Luo, Y.: Microbial models with data-driven parameters predict  
819 stronger soil carbon responses to climate change, Glob. Chang. Biol., 21(6), 2439–2453,  
820 doi:10.1111/gcb.12827, 2015.

821 Hastings, W. K.: Monte carlo sampling methods using Markov chains and their applications,  
822 Biometrika, 57(1), 97–109, doi:10.1093/biomet/57.1.97, 1970.

823 Hou, E., Lu, X., Jiang, L., Wen, D. and Luo, Y.: Quantifying Soil Phosphorus Dynamics: A Data  
824 Assimilation Approach, J. Geophys. Res. Biogeosciences, 124(7), 2159–2173,  
825 doi:10.1029/2018JG004903, 2019.

826 Ise, T. and Moorcroft, P. R.: The global-scale temperature and moisture dependencies of soil  
827 organic carbon decomposition: An analysis using a mechanistic decomposition model,  
828 Biogeochemistry, 80(3), 217–231, doi:10.1007/s10533-006-9019-5, 2006.

829 Iversen, C. M., McCormack, M. L., Powell, A. S., Blackwood, C. B., Freschet, G. T., Kattge, J.,  
830 Roumet, C., Stover, D. B., Soudzilovskaia, N. A., Valverde-Barrantes, O. J., van Bodegom, P.  
831 M. and Violle, C.: A global Fine-Root Ecology Database to address below-ground challenges in

832 plant ecology, *New Phytol.*, 215(1), 15–26, doi:10.1111/nph.14486, 2017.

833 Jiang, J., Huang, Y., Ma, S., Stacy, M., Shi, Z., Ricciuto, D. M., Hanson, P. J. and Luo, Y.:

834 Forecasting Responses of a Northern Peatland Carbon Cycle to Elevated CO<sub>2</sub> and a Gradient of

835 Experimental Warming, *J. Geophys. Res. Biogeosciences*, 123(3), 1057–1071,

836 doi:10.1002/2017JG004040, 2018.

837 Kattge, J., Bönisch, G., Díaz, S., Lavorel, S., Prentice, I. C., Leadley, P., Tautenhahn, S., Werner,

838 G. D. A., Aakala, T., Abedi, M., Acosta, A. T. R., Adamidis, G. C., Adamson, K., Aiba, M.,

839 Albert, C. H., Alcántara, J. M., Alcázar C, C., Aleixo, I., Ali, H., Amiaud, B., Ammer, C.,

840 Amoroso, M. M., Anand, M., Anderson, C., Anten, N., Antos, J., Apgaua, D. M. G., Ashman, T.

841 L., Asmara, D. H., Asner, G. P., Aspinwall, M., Atkin, O., Aubin, I., Bastrup-Spohr, L.,

842 Bahalkeh, K., Bahn, M., Baker, T., Baker, W. J., Bakker, J. P., Baldocchi, D., Baltzer, J.,

843 Banerjee, A., Baranger, A., Barlow, J., Barneche, D. R., Baruch, Z., Bastianelli, D., Battles, J.,

844 Bauerle, W., Bauters, M., Bazzato, E., Beckmann, M., Beeckman, H., Beierkuhnlein, C., Bekker,

845 R., Belfry, G., Belluau, M., Beloiu, M., Benavides, R., Benomar, L., Berdugo-Lattke, M. L.,

846 Berenguer, E., Bergamin, R., Bergmann, J., Bergmann Carlucci, M., Berner, L., Bernhardt-

847 Römermann, M., Bigler, C., Bjorkman, A. D., Blackman, C., Blanco, C., Blonder, B.,

848 Blumenthal, D., Bocanegra-González, K. T., Boeckx, P., Bohlman, S., Böhning-Gaese, K.,

849 Boisvert-Marsh, L., Bond, W., Bond-Lamberty, B., Boom, A., Boonman, C. C. F., Bordin, K.,

850 Boughton, E. H., Boukili, V., Bowman, D. M. J. S., Bravo, S., Brendel, M. R., Broadley, M. R.,

851 Brown, K. A., Bruelheide, H., Brunnich, F., Bruun, H. H., Bruy, D., Buchanan, S. W., Bucher,

852 S. F., Buchmann, N., Buitenwerf, R., Bunker, D. E., et al.: TRY plant trait database – enhanced

853 coverage and open access, *Glob. Chang. Biol.*, 26(1), 119–188, doi:10.1111/gcb.14904, 2020.

854 De Kauwe, M. G., Medlyn, B. E., Walker, A. P., Zaehle, S., Asao, S., Guenet, B., Harper, A. B.,

855 Hickler, T., Jain, A. K., Luo, Y., Lu, X., Luus, K., Parton, W. J., Shu, S., Wang, Y. P., Werner,  
856 C., Xia, J., Pendall, E., Morgan, J. A., Ryan, E. M., Carrillo, Y., Dijkstra, F. A., Zelikova, T. J.  
857 and Norby, R. J.: Challenging terrestrial biosphere models with data from the long-term  
858 multifactor Prairie Heating and CO<sub>2</sub> Enrichment experiment, *Glob. Chang. Biol.*, 23(9), 3623–  
859 3645, doi:10.1111/gcb.13643, 2017.

860 Keenan, T. F., Davidson, E., Moffat, A. M., Munger, W. and Richardson, A. D.: Using model-data  
861 fusion to interpret past trends, and quantify uncertainties in future projections, of terrestrial  
862 ecosystem carbon cycling, *Glob. Chang. Biol.*, 18(8), 2555–2569, doi:10.1111/j.1365-  
863 2486.2012.02684.x, 2012.

864 Keenan, T. F., Davidson, E. A., Munger, J. W. and Richardson, A. D.: Rate my data: Quantifying  
865 the value of ecological data for the development of models of the terrestrial carbon cycle, *Ecol.*  
866 *Appl.*, 23(1), 273–286, doi:10.1890/12-0747.1, 2013.

867 Lawrence, D. M., Fisher, R. A., Koven, C. D., Oleson, K. W., Swenson, S. C., Bonan, G., Collier,  
868 N., Ghimire, B., van Kampenhout, L., Kennedy, D., Kluzek, E., Lawrence, P. J., Li, F., Li, H.,  
869 Lombardozzi, D., Riley, W. J., Sacks, W. J., Shi, M., Vertenstein, M., Wieder, W. R., Xu, C.,  
870 Ali, A. A., Badger, A. M., Bisht, G., van den Broeke, M., Brunke, M. A., Burns, S. P., Buzan, J.,  
871 Clark, M., Craig, A., Dahlin, K., Drewniak, B., Fisher, J. B., Flanner, M., Fox, A. M., Gentine,  
872 P., Hoffman, F., Keppel-Aleks, G., Knox, R., Kumar, S., Lenaerts, J., Leung, L. R., Lipscomb,  
873 W. H., Lu, Y., Pandey, A., Pelletier, J. D., Perket, J., Randerson, J. T., Ricciuto, D. M.,  
874 Sanderson, B. M., Slater, A., Subin, Z. M., Tang, J., Thomas, R. Q., Val Martin, M. and Zeng,  
875 X.: The Community Land Model Version 5: Description of New Features, Benchmarking, and  
876 Impact of Forcing Uncertainty, *J. Adv. Model. Earth Syst.*, 11(12), 4245–4287,  
877 doi:10.1029/2018MS001583, 2019.

878 LeBauer, D. S., Wang, D., Richter, K. T., Davidson, C. C. and Dietze, M. C.: Facilitating feedbacks  
879 between field measurements and ecosystem models, *Ecol. Monogr.*, 83(2), 133–154,  
880 doi:10.1890/12-0137.1, 2013.

881 Levenberg, K.: A method for the solution of certain non-linear problems in least squares, *Q. Appl.*  
882 *Math.*, 2(2), 164–168, 1944.

883 Li, Q., Lu, X., Wang, Y., Huang, X., Cox, P. M. and Luo, Y.: Leaf area index identified as a major  
884 source of variability in modeled CO<sub>2</sub> fertilization, *Biogeosciences*, 15(22), 6909–6925,  
885 doi:10.5194/bg-15-6909-2018, 2018.

886 Liang, J., Zhou, Z., Huo, C., Shi, Z., Cole, J. R., Huang, L., Konstantinidis, K. T., Li, X., Liu, B.,  
887 Luo, Z., Penton, C. R., Schuur, E. A. G., Tiedje, J. M., Wang, Y. P., Wu, L., Xia, J., Zhou, J. and  
888 Luo, Y.: More replenishment than priming loss of soil organic carbon with additional carbon  
889 input, *Nat. Commun.*, 9(1), 1–9, doi:10.1038/s41467-018-05667-7, 2018a.

890 Liang, J., Zhou, Z., Huo, C., Shi, Z., Cole, J. R., Huang, L., Konstantinidis, K. T., Li, X., Liu, B.,  
891 Luo, Z., Penton, C. R., Schuur, E. A. G., Tiedje, J. M., Wang, Y., Wu, L. and Xia, J.: organic  
892 carbon with additional carbon input, *Nat. Commun.*, 1–9, doi:10.1038/s41467-018-05667-7,  
893 2018b.

894 Lu, D., Ricciuto, D., Walker, A., Safta, C. and Munger, W.: Bayesian calibration of terrestrial  
895 ecosystem models: A study of advanced Markov chain Monte Carlo methods, *Biogeosciences*,  
896 14(18), 4295–4314, doi:10.5194/bg-14-4295-2017, 2017.

897 Lu, D., Ricciuto, D., Stoyanov, M. and Gu, L.: Calibration of the E3SM Land Model Using  
898 Surrogate-Based Global Optimization, *J. Adv. Model. Earth Syst.*, 10(6), 1337–1356,  
899 doi:10.1002/2017MS001134, 2018.

900 Luo, Y. and Schuur, E. A. G.: Model parameterization to represent processes at unresolved scales

901 and changing properties of evolving systems, *Glob. Chang. Biol.*, 26(3), 1109–1117,  
902 doi:10.1111/gcb.14939, 2020.

903 Luo, Y., Wu, L., Andrews, J. A., White, L., Matamala, R., Schäfer, K. V. R. and Schlesinger, W.  
904 H.: ELEVATED CO<sub>2</sub> DIFFERENTIATES ECOSYSTEM CARBON PROCESSES:  
905 DECONVOLUTION ANALYSIS OF DUKE FOREST FACE DATA, *Ecol. Monogr.*, 71(3),  
906 357–376, doi:10.1890/0012-9615(2001)071[0357:ECDECP]2.0.CO;2, 2001.

907 Luo, Y., Ogle, K., Tucker, C., Fei, S., Gao, C., LaDeau, S., Clark, J. S. and Schimel, D. S.:  
908 Ecological forecasting and data assimilation in a data-rich era, *Ecol. Appl.*, 21(5), 1429–1442,  
909 doi:10.1890/09-1275.1, 2011.

910 Ma, S., Jiang, J., Huang, Y., Shi, Z., Wilson, R. M., Ricciuto, D., Sebestyen, S. D., Hanson, P. J.  
911 and Luo, Y.: Data-Constrained Projections of Methane Fluxes in a Northern Minnesota Peatland  
912 in Response to Elevated CO<sub>2</sub> and Warming, *J. Geophys. Res. Biogeosciences*, 122(11), 2841–  
913 2861, doi:10.1002/2017JG003932, 2017.

914 Metropolis, N., Rosenbluth, A. W., Rosenbluth, M. N., Teller, A. H. and Teller, E.: Equation of  
915 state calculations by fast computing machines, *J. Chem. Phys.*, 21(6), 1087–1092,  
916 doi:10.1063/1.1699114, 1953.

917 Mitchell, J. C. and Apt, K.: Concepts in programming languages, Cambridge University Press.,  
918 2003.

919 Nerger, L. and Hiller, W.: Software for ensemble-based data assimilation systems-Implementation  
920 strategies and scalability, *Comput. Geosci.*, 55, 110–118, doi:10.1016/j.cageo.2012.03.026,  
921 2013.

922 Van Oijen, M., Cameron, D. R., Butterbach-Bahl, K., Farahbakhshazad, N., Jansson, P. E., Kiese,  
923 R., Rahn, K. H., Werner, C. and Yeluripati, J. B.: A Bayesian framework for model calibration,

924 comparison and analysis: Application to four models for the biogeochemistry of a Norway  
925 spruce forest, *Agric. For. Meteorol.*, 151(12), 1609–1621, doi:10.1016/j.agrformet.2011.06.017,  
926 2011.

927 Ono, S. and Konno, T.: Estimation of flowering date and temperature characteristics of fruit trees by  
928 DTS method, *Japan Agric. Res. Q.*, 33(2), 105–108, 1999.

929 Raeder, K., Anderson, J. L., Collins, N., Hoar, T. J., Kay, J. E., Lauritzen, P. H. and Pincus, R.:  
930 DART/CAM: An ensemble data assimilation system for CESM atmospheric models, *J. Clim.*,  
931 25(18), 6304–6317, doi:10.1175/JCLI-D-11-00395.1, 2012.

932 Raupach, M. R., Rayner, P. J., Barrett, D. J., Defries, R. S., Heimann, M., Ojima, D. S., Quegan, S.  
933 and Schmullius, C. C.: Model-data synthesis in terrestrial carbon observation: Methods, data  
934 requirements and data uncertainty specifications, *Glob. Chang. Biol.*, 11(3), 378–397,  
935 doi:10.1111/j.1365-2486.2005.00917.x, 2005.

936 Rayner, P. J., Scholze, M., Knorr, W., Kaminski, T., Giering, R. and Widmann, H.: Two decades of  
937 terrestrial carbon fluxes from a carbon cycle data assimilation system (CCDAS), *Global  
938 Biogeochem. Cycles*, 19(2), n/a-n/a, doi:10.1029/2004GB002254, 2005.

939 Ricciuto, D., Sargsyan, K. and Thornton, P.: The Impact of Parametric Uncertainties on  
940 Biogeochemistry in the E3SM Land Model, *J. Adv. Model. Earth Syst.*, 10(2), 297–319,  
941 doi:10.1002/2017MS000962, 2018.

942 Ricciuto, D. M., King, A. W., Dragoni, D. and Post, W. M.: Parameter and prediction uncertainty in  
943 an optimized terrestrial carbon cycle model: Effects of constraining variables and data record  
944 length, *J. Geophys. Res.*, 116(G1), G01033, doi:10.1029/2010JG001400, 2011.

945 Richardson, A. D., Williams, M., Hollinger, D. Y., Moore, D. J. P., Dail, D. B., Davidson, E. A.,  
946 Scott, N. A., Evans, R. S., Hughes, H., Lee, J. T., Rodrigues, C. and Savage, K.: Estimating

947 parameters of a forest ecosystem C model with measurements of stocks and fluxes as joint  
948 constraints, *Oecologia*, 164(1), 25–40, doi:10.1007/s00442-010-1628-y, 2010.

949 Richardson, A. D., Hufkens, K., Milliman, T., Aubrecht, D. M., Chen, M., Gray, J. M., Johnston,  
950 M. R., Keenan, T. F., Klosterman, S. T., Kosmala, M., Melaas, E. K., Friedl, M. A. and Frolking,  
951 S.: Tracking vegetation phenology across diverse North American biomes using PhenoCam  
952 imagery, *Sci. Data*, 5, 1–24, doi:10.1038/sdata.2018.28, 2018.

953 Ridler, M. E., Van Velzen, N., Hummel, S., Sandholt, I., Falk, A. K., Heemink, A. and Madsen, H.:  
954 Data assimilation framework: Linking an open data assimilation library (OpenDA) to a widely  
955 adopted model interface (OpenMI), *Environ. Model. Softw.*, 57, 76–89,  
956 doi:10.1016/j.envsoft.2014.02.008, 2014.

957 Robert, C. and Casella, G.: *Monte Carlo statistical methods*, Springer Science & Business Media.,  
958 2013.

959 Roberts, G. O., Gelman, A. and Gilks, W. R.: Weak convergence and optimal scaling of random  
960 walk Metropolis algorithms, *Ann. Appl. Probab.*, 7(1), 110–120,  
961 doi:10.1214/AOAP/1034625254, 1997.

962 Safta, C., Ricciuto, D. M., Sargsyan, K., Debusschere, B., Najm, H. N., Williams, M. and Thornton,  
963 P. E.: Global sensitivity analysis, probabilistic calibration, and predictive assessment for the data  
964 assimilation linked ecosystem carbon model, *Geosci. Model Dev.*, 8(7), 1899–1918,  
965 doi:10.5194/gmd-8-1899-2015, 2015.

966 Scholze, M., Kaminski, T., Rayner, P., Knorr, W. and Giering, R.: Propagating uncertainty through  
967 prognostic carbon cycle data assimilation system simulations, *J. Geophys. Res.*, 112(D17),  
968 D17305, doi:10.1029/2007JD008642, 2007.

969 Shi, Z., Crowell, S., Luo, Y. and Moore, B.: Model structures amplify uncertainty in predicted soil

970 carbon responses to climate change, *Nat. Commun.*, 9(1), 1–11, doi:10.1038/s41467-018-04526-  
971 9, 2018.

972 Smith, M. J., Purves, D. W., Vanderwel, M. C., Lyutsarev, V. and Emmott, S.: The climate  
973 dependence of the terrestrial carbon cycle, including parameter and structural uncertainties,  
974 *Biogeosciences*, 10(1), 583–606, doi:10.5194/bg-10-583-2013, 2013.

975 Strigul, N., Pristinski, D., Purves, D., Dushoff, J. and Pacala, S.: Scaling from trees to forests:  
976 Tractable macroscopic equations for forest dynamics, *Ecol. Monogr.*, 78(4), 523–545,  
977 doi:10.1890/08-0082.1, 2008.

978 Tao, F., Zhou, Z., Huang, Y., Li, Q., Lu, X., Ma, S., Huang, X., Liang, Y., Hugelius, G., Jiang, L.,  
979 Doughty, R., Ren, Z. and Luo, Y.: Deep Learning Optimizes Data-Driven Representation of Soil  
980 Organic Carbon in Earth System Model Over the Conterminous United States, *Front. Big Data*,  
981 3(June), 1–15, doi:10.3389/fdata.2020.00017, 2020.

982 Trudinger, C. M., Raupach, M. R., Rayner, P. J., Kattge, J., Liu, Q., Park, B., Reichstein, M.,  
983 Renzullo, L., Richardson, A. D., Roxburgh, S. H., Styles, J., Wang, Y. P., Briggs, P., Barrett, D.  
984 and Nikolova, S.: OptIC project: An intercomparison of optimization techniques for parameter  
985 estimation in terrestrial biogeochemical models, *J. Geophys. Res. Biogeosciences*, 112(2), 1–17,  
986 doi:10.1029/2006JG000367, 2007.

987 Wang, Y. P., Trudinger, C. M. and Enting, I. G.: A review of applications of model-data fusion to  
988 studies of terrestrial carbon fluxes at different scales, *Agric. For. Meteorol.*, 149(11), 1829–1842,  
989 doi:10.1016/j.agrformet.2009.07.009, 2009.

990 Weng, E. and Luo, Y.: Relative information contributions of model vs. data to short- and long-term  
991 forecasts of forest carbon dynamics, *Ecol. Appl.*, 21(5), 1490–1505, doi:10.1890/09-1394.1,  
992 2011.

993 Weng, E., Dybzinski, R., Farrior, C. E. and Pacala, S. W.: Competition alters predicted forest  
994 carbon cycle responses to nitrogen availability and elevated CO<sub>2</sub>: simulations using an explicitly  
995 competitive, game-theoretic vegetation demographic model, *Biogeosciences Discuss.*, 1–35,  
996 doi:10.5194/bg-2019-55, 2019.

997 Williams, M., Schwarz, P. A., Law, B. E., Irvine, J. and Kurpius, M. R.: An improved analysis of  
998 forest carbon dynamics using data assimilation, *Glob. Chang. Biol.*, 11(1), 89–105,  
999 doi:10.1111/j.1365-2486.2004.00891.x, 2005.

1000 Williams, M., Richardson, A. D., Reichstein, M., Stoy, P. C., Peylin, P., Verbeeck, H., Carvalhais,  
1001 N., Jung, M., Hollinger, D. Y., Kattge, J., Leuning, R., Luo, Y., Tomelleri, E., Trudinger, C. M.  
1002 and Wang, Y. P.: Improving land surface models with FLUXNET data, *Biogeosciences*, 6(7),  
1003 1341–1359, doi:10.5194/bg-6-1341-2009, 2009.

1004 Xu, T., White, L., Hui, D. and Luo, Y.: Probabilistic inversion of a terrestrial ecosystem model:  
1005 Analysis of uncertainty in parameter estimation and model prediction, *Global Biogeochem.  
1006 Cycles*, 20(2), 1–15, doi:10.1029/2005GB002468, 2006.

1007 Yun, K., Hsiao, J., Jung, M. P., Choi, I. T., Glenn, D. M., Shim, K. M. and Kim, S. H.: Can a multi-  
1008 model ensemble improve phenology predictions for climate change studies?, *Ecol. Modell.*, 362,  
1009 54–64, doi:10.1016/j.ecolmodel.2017.08.003, 2017.

1010 Zobitz, J. M., Desai, A. R., Moore, D. J. P. and Chadwick, M. A.: A primer for data assimilation  
1011 with ecological models using Markov Chain Monte Carlo (MCMC), *Oecologia*, 167(3), 599–  
1012 611, doi:10.1007/s00442-011-2107-9, 2011.

1013

Table1: Comparison among MIDA and available DA tools

DA tool	Agnostic	DA algorithms	Global optima	Posterior distribution	Visualization
CCDAS	No	Automatic differentiation from Transformation of Algorithms in Fortran (TAF)	No	No	No
CARDAMOM	No	Markov Chain Monte Carlo	Yes	Yes	No
EcoPAD	No	Markov Chain Monte Carlo	Yes	Yes	Yes
OpenDA	No	EnKF, Ensemble Square-Root Filter, Particle Filter	Yes	Yes	No
DART	Yes	EnKF	Yes	Yes	No
PDAF	Yes	EnKF	Yes	Yes	No
PEST	Yes	Levenberg-Marquardt method	Rely on initial parameter values	No	No
MIDA	Yes	Markov Chain Monte Carlo	Yes	Yes	Yes

Table 2: A summary of 21 parameters to be calibrated in DALEC model. The default parameter value and prior parameter range are shown.

<b>Parameter</b>	<b>Description</b>	<b>Unit</b>	<b>Default</b>	<b>Range</b>
$GDD_{min}$	Growing degree day threshold for leaf out	$^{\circ}C\ d$	100	[10, 250]
$GDD_{max}$	Growing degree day threshold for maximum LAI	$^{\circ}C\ d$	200	[50, 500]
$LAI_{max}$	Seasonal maximum leaf area index	-	4	[2, 7]
$T_{leaffall}$	Temperature for leaf fall	$^{\circ}C$	5	[0, 10]
$K_{leaf}$	Rate of leaf fall	$d^{-1}$	0.1	[0.03, 0.95]
$NUE$	N use efficiency	-	7	[1, 20]
$Res_{growth}$	Growth respiration fraction	-	0.2	[0.05, 0.5]
$Res_m$	Base rate for maintenance respiration	$\times 10^{-4}\ \mu mol\ m^{-2}d^{-1}$	1	[0.1, 100]
$Q_{10_{mr}}$	Maintenance respiration T-sensitivity	-	2	[1, 4]
$A_{stem}$	Allocation to plant stem pool	-	0.7	[0.1, 0.95]
$\tau_{root}$	Root turnover time	$\times 10^{-4}\ d^{-1}$	5.48	[1.1, 27.4]
$\tau_{stem}$	Stem turnover time	$\times 10^{-5}\ d^{-1}$	5.48	[1.1, 27.4]
$Q_{10_{hr}}$	Heterotrophic respiration T-sensitivity	-	2	[1, 4]
$\tau_{litter}$	Base turnover for litter	$\times 10^{-3}\ umol\ m^{-2}d^{-1}$	1.37	[0.548, 5.48]
$\tau_{som}$	Base turnover for soil organic matter	$\times 10^{-4}\ umol\ m^{-2}d^{-1}$	9.13	[0.274, 2.74]
$K_{decomp}$	Decomposition rate	$\times 10^{-3}\ d^{-1}$	1	[0.1, 10]
$LMA$	Leaf mass per area	$gC\ m^{-2}$	80	[20, 150]
$X_{stem_{init}}$	Initial value for stem C pool	$\times 10^3\ gC$	5	[1, 15]
$X_{root_{init}}$	Initial value for root C pool	$gC$	500	[100, 3000]
$X_{litter_{init}}$	Initial value for litter C pool	$gC$	600	[50, 1000]
$X_{som_{init}}$	Initial value for soil organic C pool	$\times 10^3\ gC$	7	[1, 25]

Table 3: A summary of eight parameters to be calibrated in surrogate-based ELM model. The default parameter value and prior parameter range are shown.

Parameter	Description	Unit	Default	Range
$c_{root}$	Rooting depth distribution parameter	$m^{-1}$	2.0	[0.5, 4]
$SLA_{top}$	Specific leaf area at canopy top	$m^2 gC^{-1}$	0.03	[0.01, 0.05]
$N_{leaf}$	Fraction of leaf N in RuBisCO	-	0.1007	[0.1, 0.4]
$CN_{root}$	Fine root C:N ratio	-	42	[25, 60]
$A_{r2l}$	Allocation ratio of fine root to leaf	-	1.0	[0.3, 1.5]
$Res_m$	Base rate for maintenance respiration	$\times 10^{-6} \mu mol m^{-2} s^{-1}$	2.525	[1.5, 4]
$t_{leaffall}$	Critical day length for senescence	$\times 10^4$ s	3.93	[3.5, 4.5]
$GDD_{onset}$	Accumulated growing degree days for leaf out	$^{\circ}C d$	800	[600, 1000]

Table 4: A summary of two parameters to be calibrated in the BiomE model. The default parameter value and prior parameter range are shown.

Parameter	Description	Unit	Default	Range
$V_{annual}$	Annual productivity per unit leaf area	$kgC\ y^{-1}m^2$	0.4	[0.2, 2]
$M_{canopy}$	Annual mortality rate in canopy layer	$y^{-1}$	0.02	[0.01, 0.08]

## Figure captions

**Figure 1:** The three-step workflow of Model Independent Data Assimilation (MIDA) module. The workflow includes data preparation, execution of data assimilation (DA), and visualization. The data preparation step is to provide all the formatted essential data for DA via user input. The execution step is to calibrate parameter values towards a constrained posterior distribution with the fusion of observations. The visualization step is to diagnose the effects of DA. Rhombus in orange represents user-input data. Rectangle represents procedures and document/multidocument shape is for data files in computers. Dashed lines indicate locations of data. Solids lines indicate data flow pathways. With the three-step workflow, DA is agnostic to specific models and users will be released from technical burdens.

**Figure 2:** the GUI-MIDA window includes two panels. The upper panel is to set up a data assimilation task. Inputs can be loaded and applied to the step 1 on data preparation for DA. The lower panel is to run DA as described in step 2 and visualize the posterior distributions of parameters in step 3.

**Figure 3:** Comparison between the simulated daily net ecosystem exchange (NEE) by DALEC and the observed NEE at Harvard Forest from 1992 to 2006. Red circles represent modeled NEE with the optimized parameter values and green circles represent simulated NEE with the original parameter values. Simulations of DALEC are substantially improved after data assimilation in comparison with those before data assimilation.

**Figure 4:** Comparison between posterior distributions (red line) and default values (gray dash line) of the 21 parameters in DALEC. The peak in posterior distribution is the constrained parameter value from maximum likelihood estimation. This distinctive mode and its divergence from the default value indicates the effects of DA. Most parameters are well constrained, and some are far different from the original values.

**Figure 5:** Comparison between posterior distributions (red line) and default values (gray dash line) of the eight parameters in surrogate-based ELM. The peak in posterior distribution is the constrained parameter value from maximum likelihood estimation. This distinctive mode and its divergence from the default value indicates the effects of DA. Most parameters are well constrained, and some are far different from the original values.

**Figure 6:** Comparison between the simulated NEE, total leaf area index, latent heat flux by surrogate-based ELM and the observed ones at Missouri Ozark flux site from 2006 to 2014. The

blue lines indicate the observations, and their 95% confidence interval is in the dashed area. The green and red lines indicate the simulations with default parameter values and optimized values respectively. Simulations are generally improved after DA for all these three variables.

**Figure 7:** Comparison between the simulated growth date by 9 phenology models after DA and the observed growth date for *Larix laricina* with +9°C treatment at SPRUCE site from 2016 to 2018. Colored number indicates different models and shape represents different year. Overall, model 6,7,8,9 achieve better performance after DA.

**Figure 8:** Comparison between posterior distributions (red line) and default values (gray dash line) of the two parameters in BiomeE. The peak in posterior distribution is the constrained parameter value from maximum likelihood estimation. This distinctive mode and its divergence from the default value indicates the effects of DA. All parameters are well constrained and different from their original values.

**Figure 9:** Comparison between the simulated leaf area index (LAI) by BiomeE and the observed NEE at Willow Creek. Circles represent modeled NEE with the optimized parameter values and triangles represent simulated NEE with the original parameter values. Simulations of LAI are substantially improved after data assimilation in comparison with those before data assimilation.

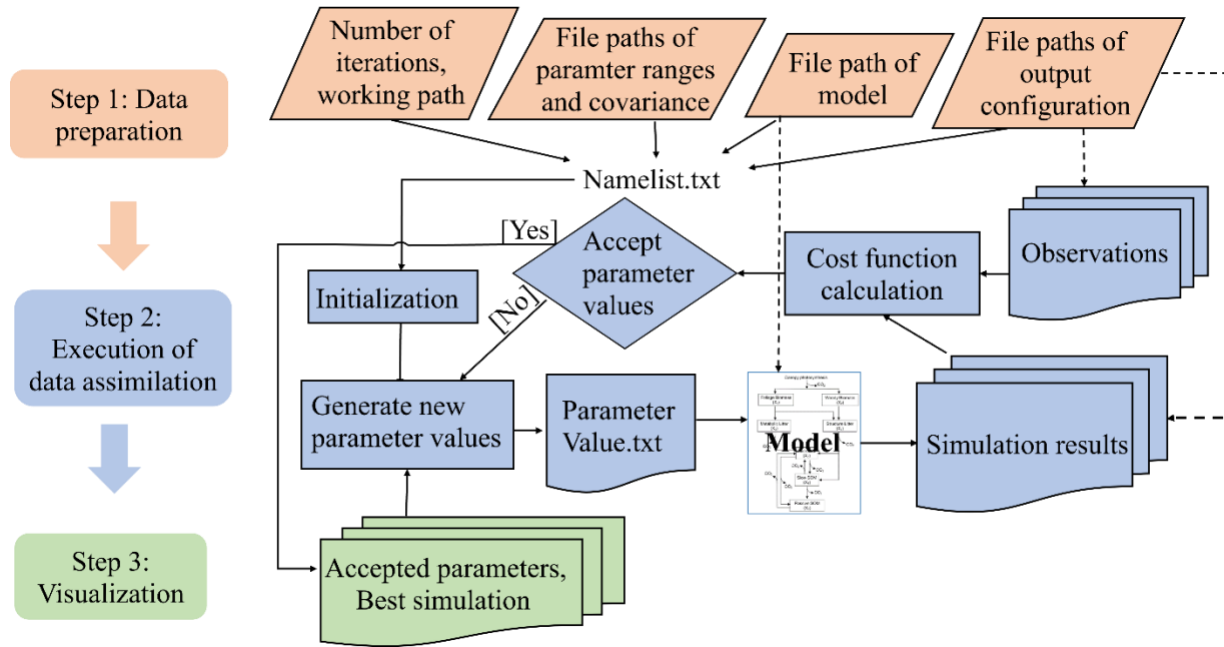


**Figure 1:** The three-step workflow of Model Independent Data Assimilation (MIDA) module. The workflow includes data preparation, execution of data assimilation (DA), and visualization. The data preparation step is to provide all the formatted essential data for DA via user input. The execution step is to calibrate parameter values towards a constrained posterior distribution with the fusion of observations. The visualization step is to diagnose the effects of DA. Rhombus in orange represents user-input data. Rectangle represents procedures and document/multidocument shape is for data files in computers. Dashed lines indicate locations of data. Solids lines indicate data flow pathways. With the three-step workflow, DA is agnostic to specific models and users will be released from technical burdens.

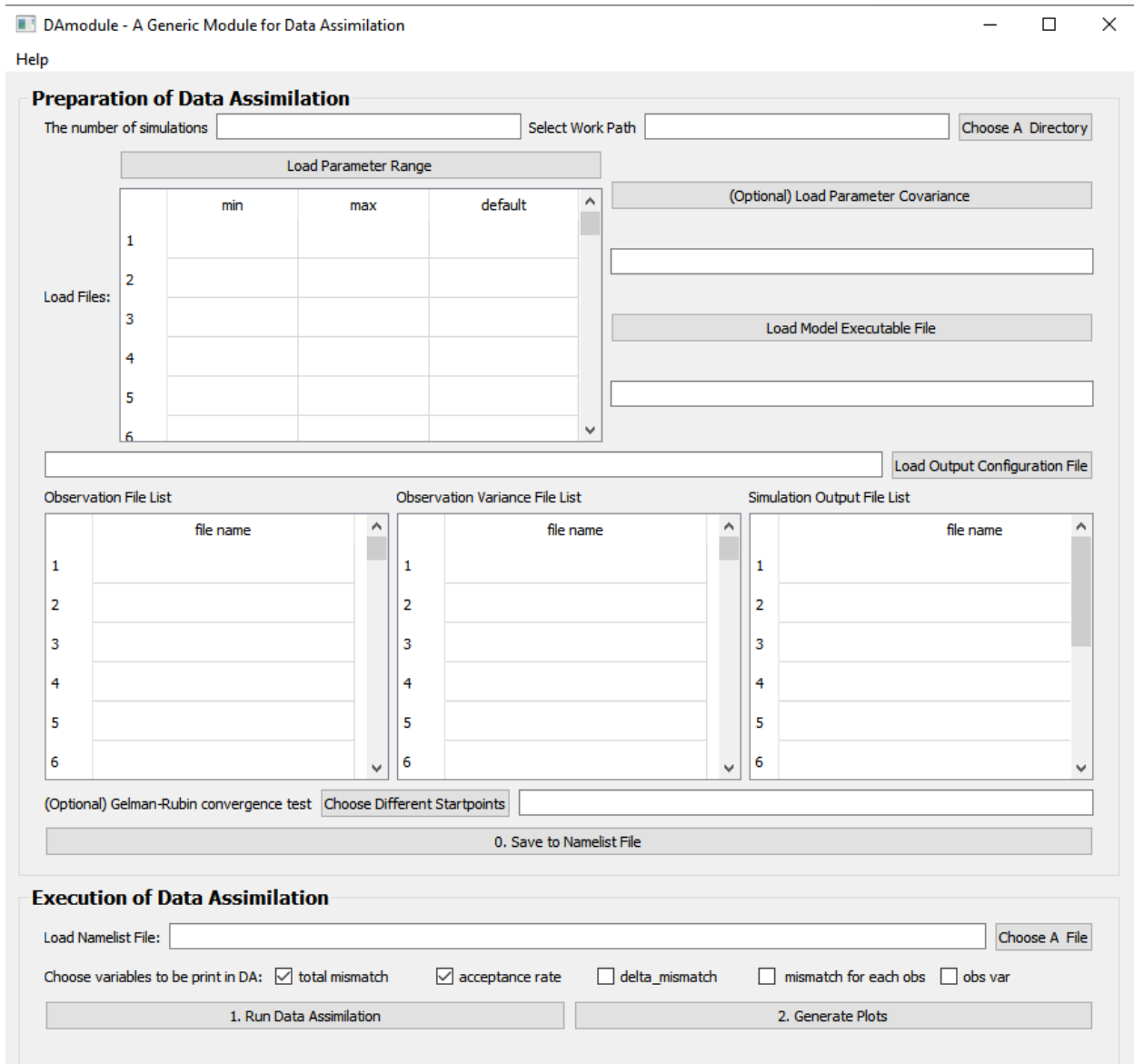


**Figure 2:** the GUI-MIDA window includes two panels. The upper panel is to set up a data assimilation task. Inputs can be loaded and applied to the step 1 on data preparation for DA. The lower panel is to run DA as described in step 2 and visualize the posterior distributions of parameters in step 3.

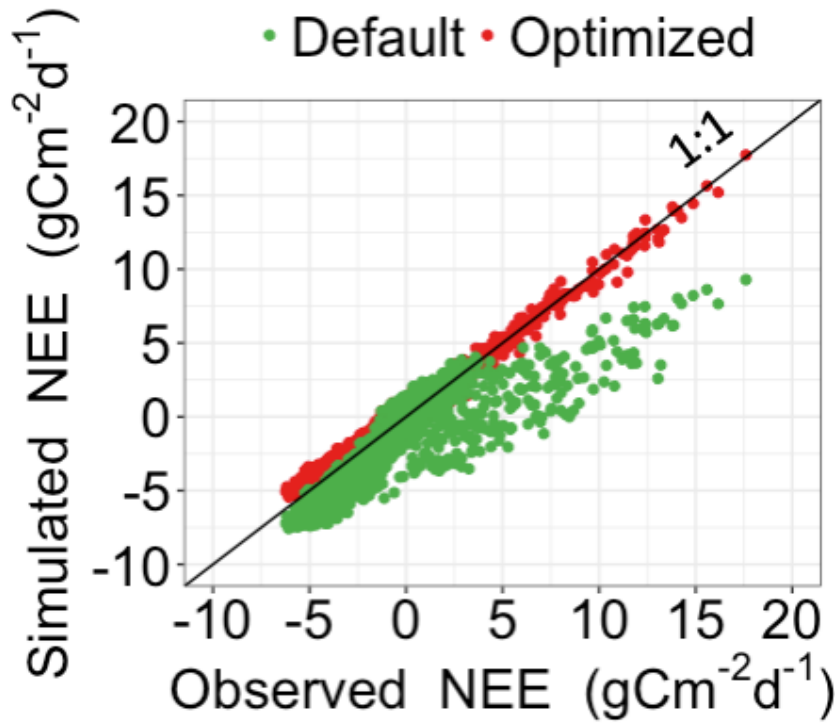


**Figure 3:** Comparison between the simulated daily net ecosystem exchange (NEE) by DALEC and the observed NEE at Harvard Forest from 1992 to 2006. Red circles represent modeled NEE with the optimized parameter values and green circles represent simulated NEE with the original parameter values. Simulations of DALEC are substantially improved after data assimilation in comparison with those before data assimilation.

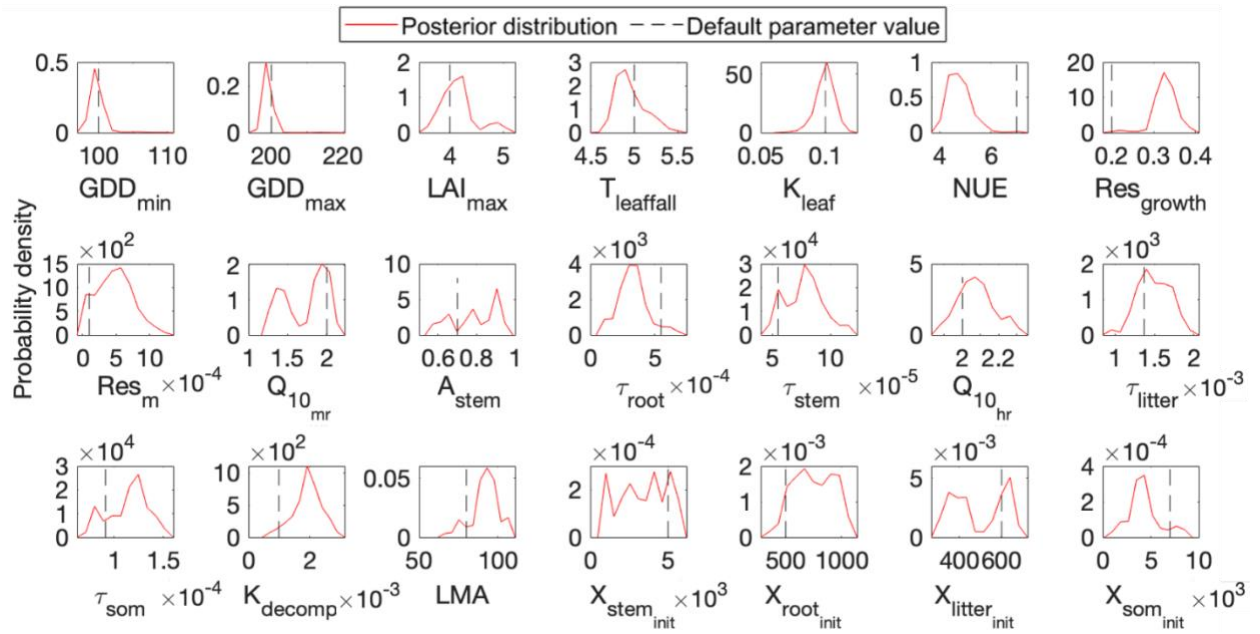


**Figure 4:** Comparison between posterior distributions (red line) and default values (gray dash line) of the 21 parameters in DALEC. The peak in posterior distribution is the constrained parameter value from maximum likelihood estimation. This distinctive mode and its divergence from the default value indicates the effects of DA. Most parameters are well constrained, and some are far different from the original values.

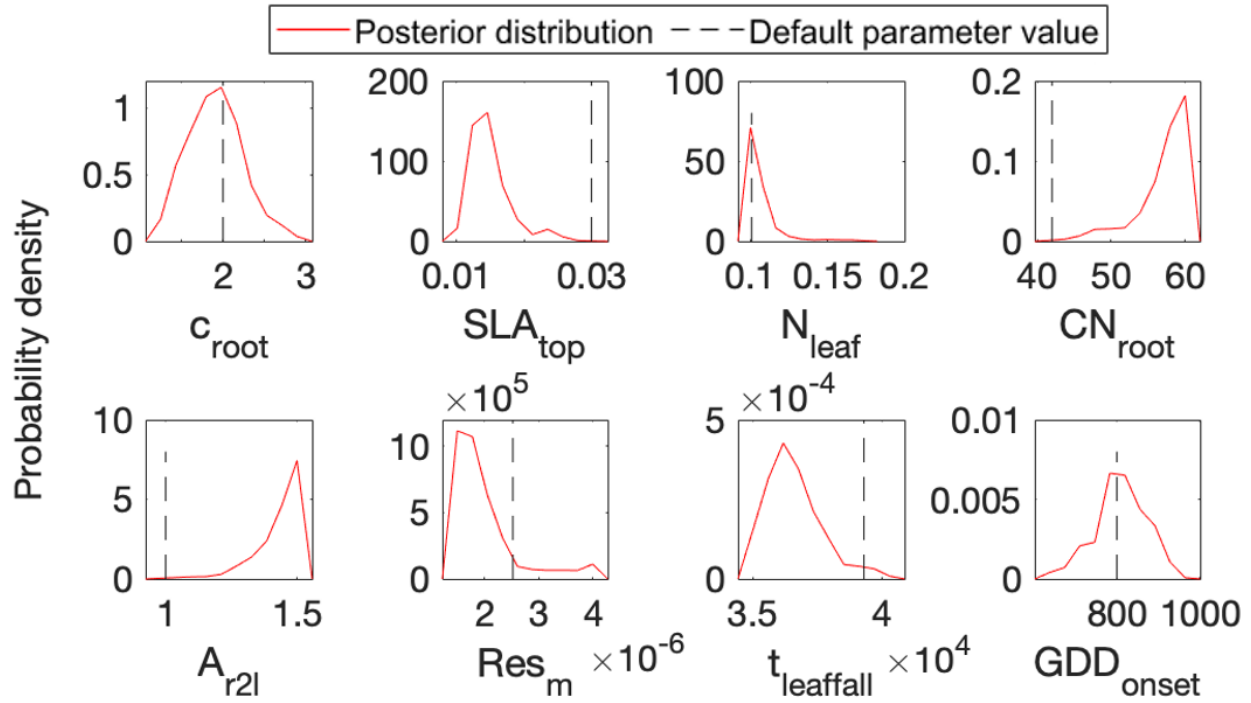


**Figure 5:** Comparison between posterior distributions (red line) and default values (gray dash line) of the eight parameters in surrogate-based ELM. The peak in posterior distribution is the constrained parameter value from maximum likelihood estimation. This distinctive mode and its divergence from the default value indicates the effects of DA. Most parameters are well constrained, and some are far different from the original values.

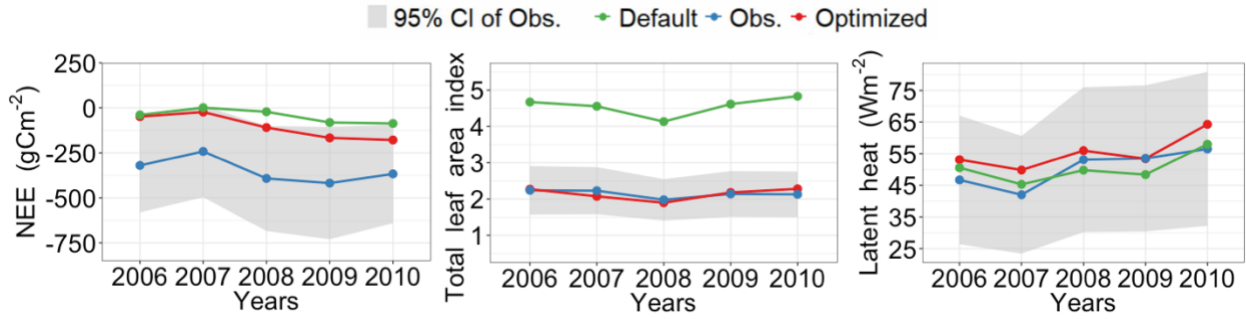


**Figure 6:** Comparison between the simulated NEE, total leaf area index, latent heat flux by surrogate-based ELM and the observed ones at Missouri Ozark flux site from 2006 to 2014. The blue lines indicate the observations, and their 95% confidence interval is in the dashed area. The green and red lines indicate the simulations with default parameter values and optimized values respectively. Simulations are generally improved after DA for all these three variables.

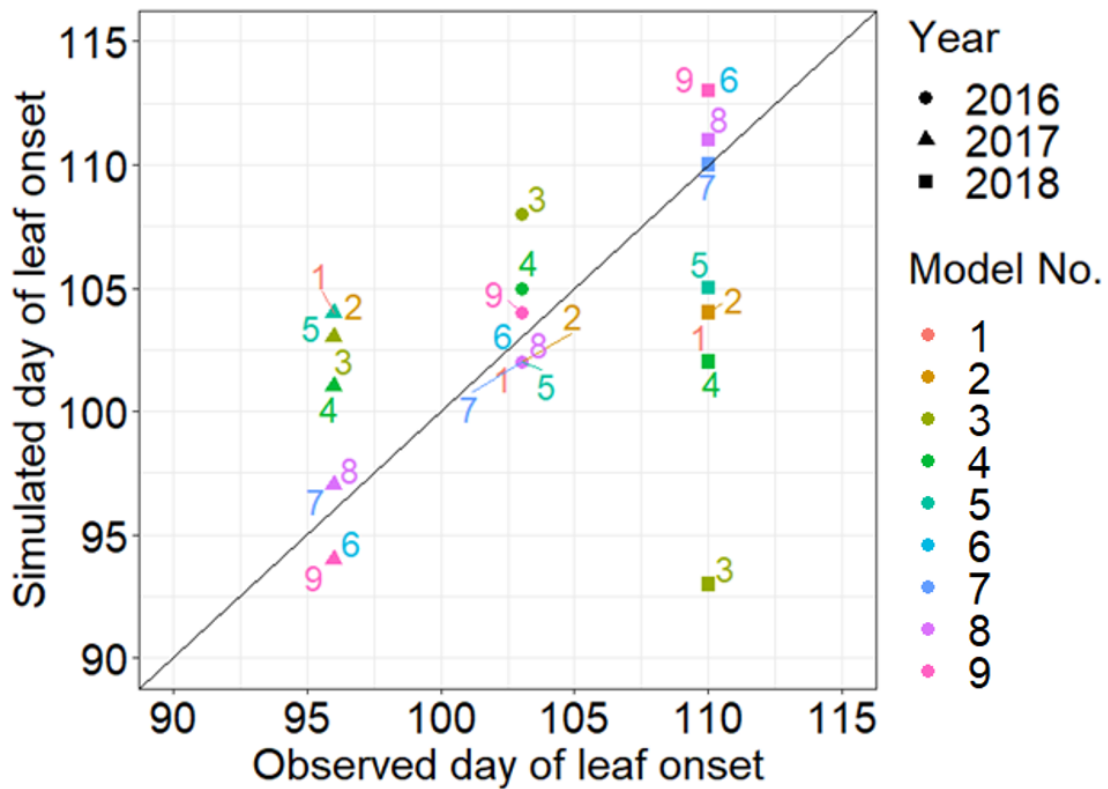


**Figure 7:** Comparison between the simulated growth date by 9 phenology models after DA and the observed growth date for *Larix laricina* with +9°C treatment at SPRUCE site from 2016 to 2018. Colored number indicates different models and shape represents different year. Overall, model 6,7,8,9 achieve better performance after DA.

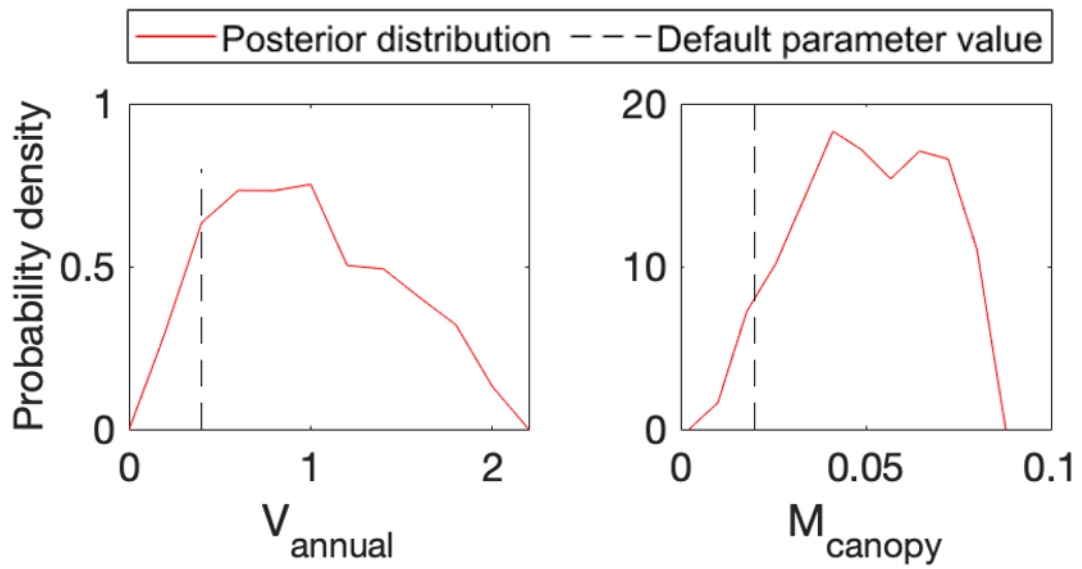


**Figure 8:** Comparison between posterior distributions (red line) and default values (gray dash line) of the two parameters in BiomeE. The peak in posterior distribution is the constrained parameter value from maximum likelihood estimation. This distinctive mode and its divergence from the default value indicates the effects of DA. All parameters are well constrained and different from their original values.

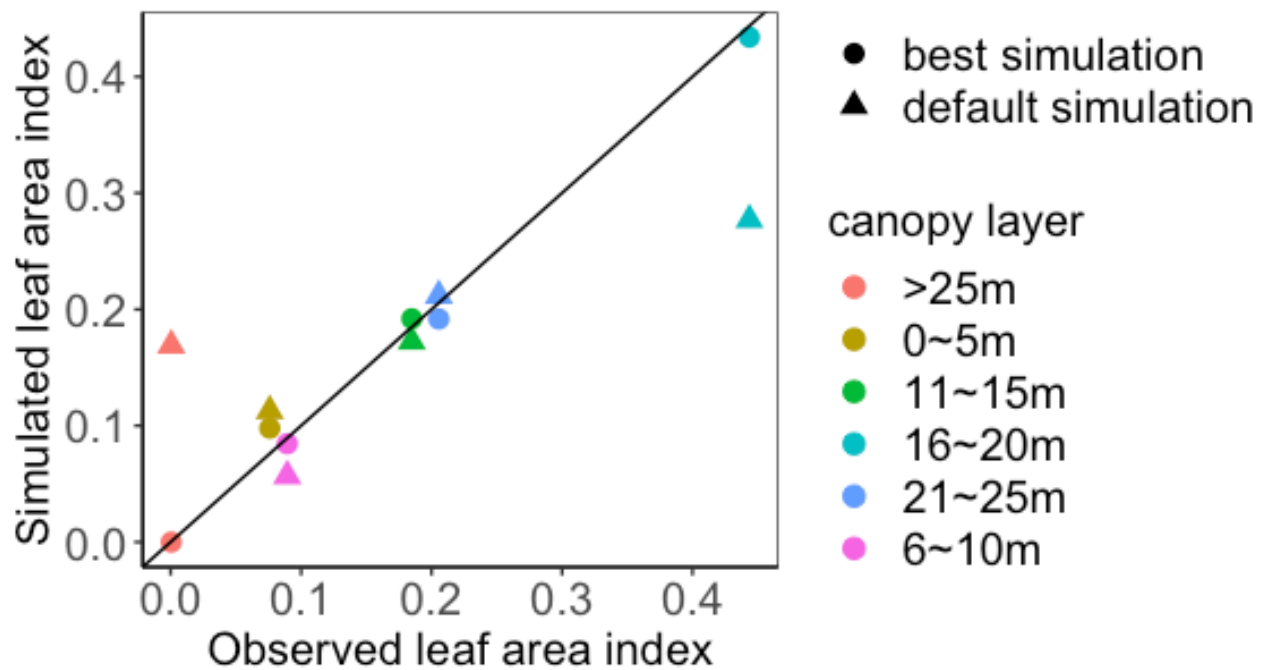


**Figure 9:** Comparison between the simulated leaf area index (LAI) by BiomeE and the observed NEE at Willow Creek. Circles represent modeled NEE with the optimized parameter values and triangles represent simulated NEE with the original parameter values. Simulations of LAI are substantially improved after data assimilation in comparison with those before data assimilation.